The High-Latitude Ionosphere and its Effects on Radio Propagation

R. D. Hunsucker, J. K. Hargreaves

Book DOI: http://dx.doi.org/10.1017/CBO9780511535758

Online ISBN: 9780511535758

Hardback ISBN: 9780521330831

Paperback ISBN: 9780521041362

Chapter

Chapter 4 - Radio techniques for probing the ionosphere pp. 181-226

Chapter DOI: http://dx.doi.org/10.1017/CBO9780511535758.006

Cambridge University Press

Chapter 4

Radio techniques for probing the ionosphere

4.1 Introduction

The purpose of this chapter is to review the basic techniques (and the newer modifications and adaptations of these techniques) for studying the terrestrial ionosphere, with particular emphasis on the capabilities and limitations of the techniques when they are used to probe the high-latitude ionosphere. We are fortunate to have several books and reports written since 1989 that have addressed the general topic of ionospheric investigations using radio techniques (Kelley, 1989; Liu, 1989; Davies, 1990; Hunsucker, 1991; Hargreaves, 1992; Hunsucker, 1993 and 1999; pp. 502–505), so in this chapter we will emphasize the limitations and capabilities of these techniques and update the information on deployment of ionospheric instrumentation at high latitudes. Figure 3.34 of Chapter 3 shows the frequency–height regimes which various selected radio techniques can probe.

4.2 Ground-based systems

4.2.1 Ionosondes

In its simplest form, an ionosonde consists of a transmitter and receiver with coupled tuning circuits, which is swept in frequency (usually in the frequency range of approximately 0.5–25 MHz). It can be either a pulsed or a CW-FM (chirp) system, and the transmitter and receiver can either be co-located (monostatic) or separated (bistatic). After the RF signals have been reflected by the ionosphere they are received and processed by the receiver to produce *ionograms.* The

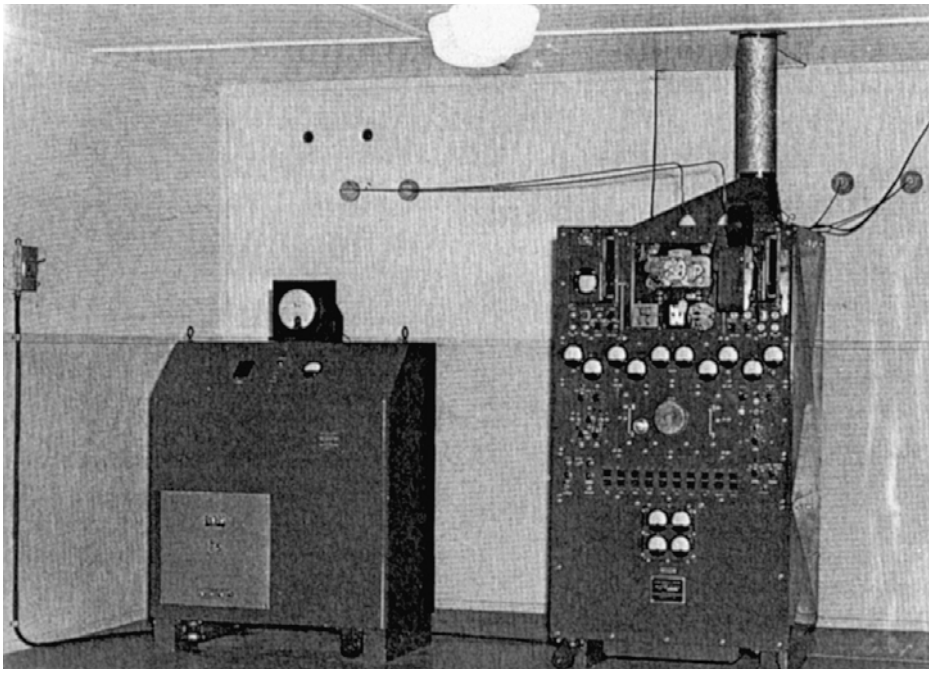

Figure 4.1. NBS Model C-3 ionosonde installation. The power supply is on the left and the actual ionosonde is on the right.

basic information in the received signal is the transit time for passage between ionospheric layers and the Earth, frequency, amplitude, phase, polarization, Doppler shift, and spectrum shape (see Section 3.2.4). From these quantities, we can obtain an *ionogram*, which is a plot of the *virtual height* of reflection versus frequency. We can also deduce the *true height* of ionospheric layers as a function of frequency, the *line-of-sight (LOS)* velocity, some communication parameters, and the vector velocity of ionospheric irregularities (with an array of several antennas). Historically, the ionosonde was the instrument used to confirm the existence of the ionosphere by Appleton and Barnett (1926) and by Breit and Tuve (1926). A brief account of the development of the primitive and first-generation ionosonde is given in Sections 3.1 and 3.2 of Hunsucker (1991) and by Bibl (1998).

The so-called "standard" ionosondes used vacuum tubes and electromechanical tuning mechanisms and were very bulky and heavy, as shown in Figure 4.1. A typical ionogram from a "standard" ionosonde in Yamagawa, Japan is shown in Figure 4.2, whereas an idealized ionogram is shown in Figure 4.3.

These standard ionosondes were produced in relatively large numbers, and were deployed globally from c. 1942 until 1975. The photographically recorded data provided by these sounders have contributed greatly to our state of knowledge of the ionosphere. The data, however, must be manually analyzed by trained "scalers" and the data film archived in controlled-climate storage facilities. A map

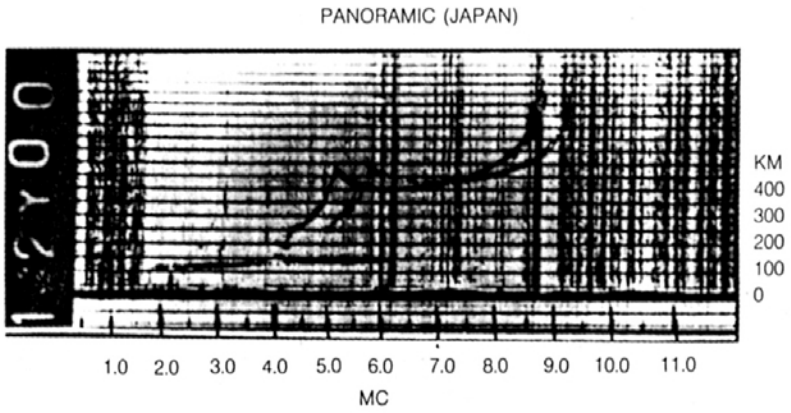

Figure 4.2. A "typical ionogram" from a "standard" ionosonde (frequency range 0.5–12 MHz , height range 1000 km, power 10 kW, sweep time 20 s, linear frequency scale. Note the heavy vertical lines – caused by MF and HF interference.

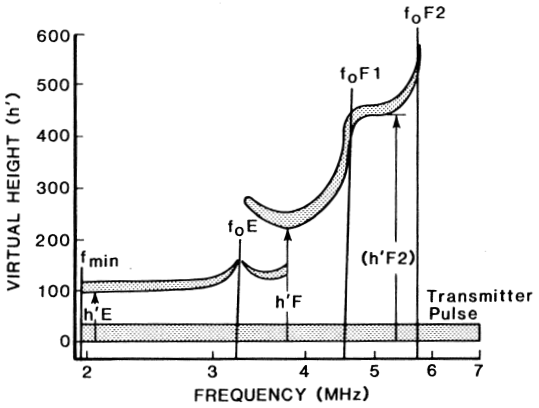

Figure 4.3. An idealized ionogram.

of the global distribution of ionosondes (mainly the standard models) as of 1982 is shown in Figure 4.4.

With the advent of reasonably priced compact personal computers, digital signal processing, new modulation-coding techniques, and VLSI, a new generation of ionosondes was developed, starting in the mid-1960s and continuing into this century. Many of these ionosondes are portable and all have much smaller volume, weight, and power consumption than did the standard ionosondes, and they produce much better ionograms. The modern sounders also permit the deletion of discrete frequencies that are contaminated by interference, and the deletion of frequencies that may interfere with other services. Advances in antenna-array theory have also made it possible to deploy arrays of receiving antennas in such a way as to permit direction-of-arrival (DOA) determination for echoes, permitting the production of "skymaps" for selected heights.

Figure 4.4. A map of all ionosondes known to have existed as of 1982.

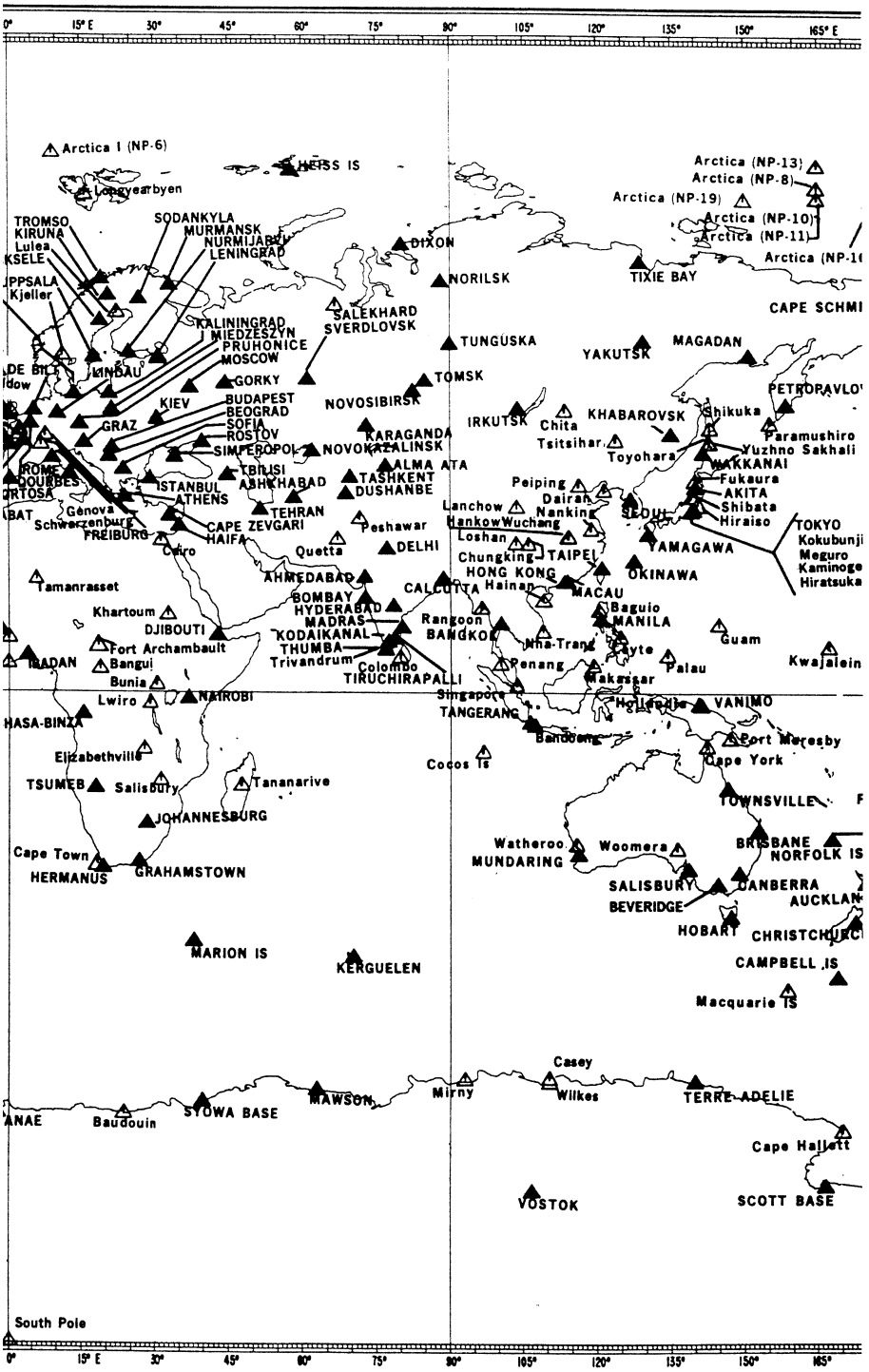

RTICAL SOUNDING STATIONS

Representative examples of the new sounders available at the time of writing are shown in Table 4.1. An ionogram obtained from a typical modern ionosonde is illustrated in Figure 4.5.

Most of the ionosondes which produce ionograms such as that shown in Figure 4.5 are of the "modern" type, since the "standard" ionosondes are obsolescent and extremely difficult to maintain. An up-to-date description of the modern sounders and their deployment is given by Wilkinson (1995). The modern ionosondes permit the study of a wide range of ionospheric irregularities as illustrated schematically in Figure 3.34.

Capabilities and limitations

A limitation of *all* ionosondes is that they can yield information on the ionosphere only up to the height of maximum ionization of the F2 layer (the "bottomside" of the ionosphere). Also, unless one extends the low-frequency end of the sweep (to at least 250 kHz) by increasing the height of the transmitting antenna tower and using relatively high power, not much information can be obtained from the D

Table 4.1. *Typical available ionosondes*

Name of Sounder	Specifications	Source
Digisonde Portable Sounder (DPS)	Frequency range 1–32 MHz Power 300 W pulse Height range 90–1000 km Doppler sounding, etc. Realtime data transfer via the internet Automatic scaling available	University of Massachusetts Center for Atmospheric Research, 600 Suffolk Street, 3rd Floor, Lowell, MA 01854, USA www.uml.edu
Canadian Advanced Digital Ionosonde (CADI)	Frequency range 1–20 MHz Power 600 W pulse (13-bit Barker code) Height range 90–1024 km Doppler sounding, etc. Realtime data transfer via the internet	Scientific Instruments, Ltd, 2233 Hanselman Avenue, Saskatoon, CA S7L6A7, USA
Ionosonde: HF Diagnostics Module, 01-2000	Frequency range 1–30 MHz Power 1 kW CW and peak Doppler sounding, etc.	Center for Remote Sensing, Inc., 11350 Random Hills Road, Suite 710, Fairfax, VA 22030, USA
Advanced Digital Ionosonde, IPS-71	For specifications contact www.kel.gov.au	KEL Aerospace Pty Ltd, 231 High Street, Ashburton, Victoria 3147, Australia

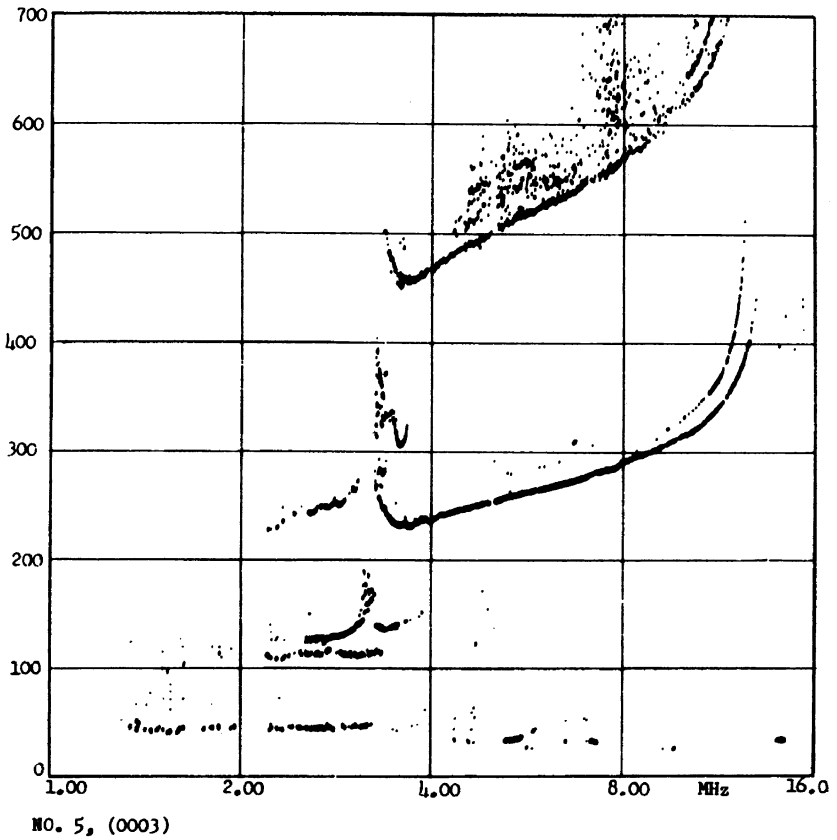

Figure 4.5. A typical modern digital ionogram (compare with Figure 4.2).

region. This is in contrast with the incoherent-scatter-radar (ISR) technique, which, however, is much more expensive and definitely not as portable. Another limitation is that, during episodes of intense E-region ionization ("blanketing-E"), it is not possible to obtain much information on the F region. Approximate costs of new "modern" ionosondes currently vary from about $ 30 000 to over $ 250 000.

At auroral latitudes *all* ionosondes are subject to several rather severe limitations – namely that, during some of the most "interesting" times, auroral-E ionization or D-region absorption precludes the gathering of any ionospheric information on the layers above! These "interesting" times include magnetic storms and substorms and associated auroral and polar-cap absorption, intense auroral events, and extreme spread-F conditions.

4.2.2 Coherent oblique-incidence radio-sounding systems

We shall refer to the systems which utilize coherent radars to obtain either direct backscatter or ground-reflected backscatter from ionospheric features as *oblique backscatter sounders* (OBSs). The systems may be either bistatic or monostatic in

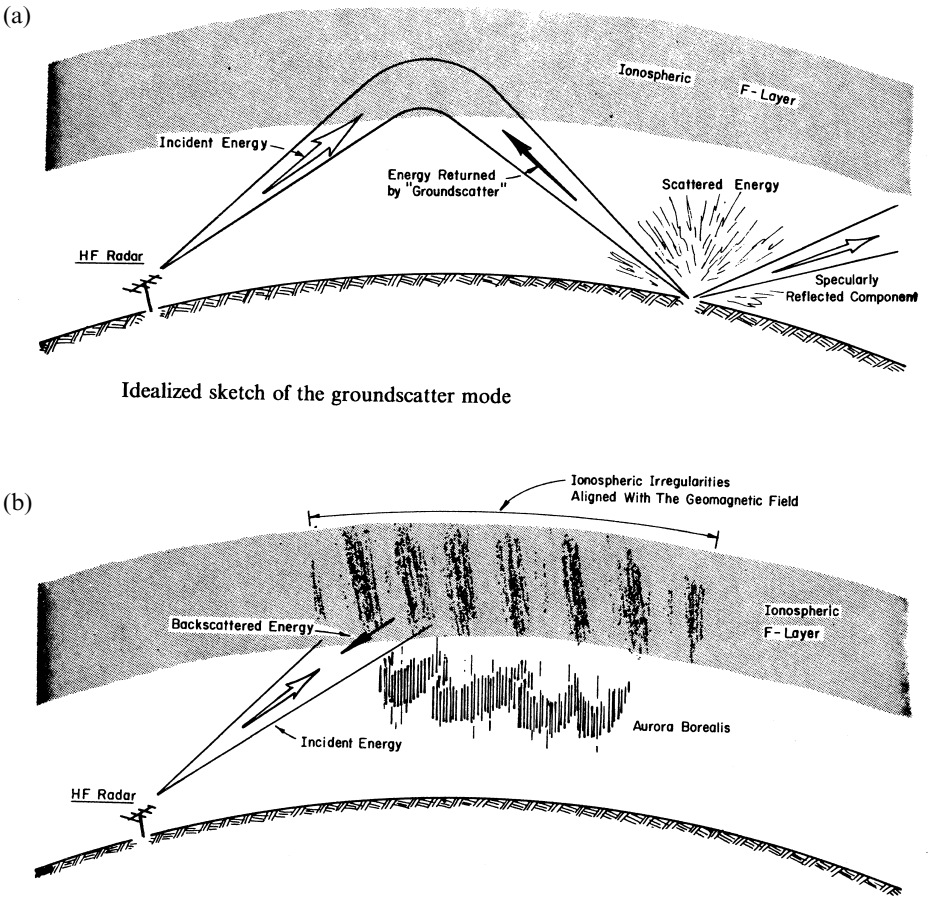

Figure 4.6. An idealized sketch of the ground backscatter mode (a) and a sketch of direct backscatter from field-aligned irregularities (FAIs) in the auroral oval (b). In reality, the HF ray path is usually refracted by the ionosphere, making it orthogonal to the FAI.

configuration. OBS systems are also referred to in the literature as *ionospheric radars, coherent scatter radars (CSRs)*, *backscatter sounders*, and *auroral radars.* They are discussed in considerable detail in Greenwald *et al.* (1978), Liu (1989, Sections 11 and 12), Hunsucker (1991, pp. 94–109), and Hunsucker (1993, pp. 441–450). Specifically, the *WITS Handbook*, edited by Liu (1989) devotes Sections 11 and 12 (64 pages) to two types of OBS systems: auroral radars and HF groundscatter radars in Appendix A1.2, as well as fundamentals of plasma dynamics and electrodynamics of the equatorial, mid-latitude, and high-latitude ionosphere in Chapters 2, 3, 5, and 6.

Basic principles

A coherent-scatter echo exhibits a statistical correlation of the amplitude and phase from one pulse to another, and emanates from quasi-deterministic gra-

dients in electron density, which have correlation times usually greater than 1 ms. One can also describe backscatter as "strong" compared with incoherent-scatter echoes (the "scattering cross-section" for coherent backscatter is 10^4–10^9 times greater than that for incoherent scatter). In general, coherent backscatter is obtained when the ray path from the transmitting antenna intersects large electron-density gradients or field-aligned irregularities, at near-perpendicular incidence. Thus, coherent backscatter is 40–90 dB stronger than incoherent scatter, and is qualitatively similar to specular reflection. However, for a full understanding of the ionospheric physics, considerable plasma theory must be employed. The essence of the plasma-theory description is that, when plasma instabilities are present in the ionosphere, the amplitude of fluctuations in the medium can grow to much higher levels than the thermal background. Coherent scatter occurs when the wave vector of the medium (k_m) equals twice the wave vector of the transmitted wave (k_t).

Rather complete descriptions of the history of the development of the OBS technique, and basics of the various systems, were given by Croft (1972), in Chapter 11 of the *WITS Handbook*, and in Hunsucker (1991, Sections 4.1.1, 4.2.1, and 4.3.1). It is interesting to note that the first observation of coherent backscatter (from the ground) was made by Mogel in 1926, but not really understood until 1951, when it was explained independently by Dieminger (1951) and Peterson (1951). There is another class of sounders known as oblique ionosondes or "synchronized-sounders," which are used primarily for assessing propagation characteristics of the ionosphere for HF communication circuits (see Goodman, 1992, Chapter 6). There is also an important "subset" of OBSs, most often referred to as over-the-horizon (OTH) radars, which are used by military services and other government agencies primarily for the detection of airplanes, ships, and missiles. The hardware and software are quite sophisticated, and the subject had been highly classified until fairly recently, when some of the systems were made available for ionospheric and oceanographic research. Descriptions of some of the OTH radar systems and results are given by Barnum (1986), Brookner (1987), in a special issue of the *IEEE Journal on Oceanic Engineering* (1986), and in a special section of *Radio Science* (1998).

Modern OBS systems typically operate in the HF and VHF bands and use continuous-wave (CW), pulse-coded, or FMCW modulation. They obtain ionospheric information either from direct backscatter from field-aligned irregularities, or by backscatter from irregularities via a ground-reflected mode, as illustrated in the idealized sketch in Figure 4.6.

In the groundscatter mode (at the top of Figure 4.6), the echoes returned to the receiver will be affected by irregularities near the ionospheric-reflection point, by the Earth-surface characteristics, and by field-aligned irregularities (FAIs), where the second hop enters the ionosphere. It is necessary to analyze the Doppler velocity, the phase characteristics, and the spectral shape of the echo to identify the scattered echo of interest. The bottom part of Figure 4.6 illustrates the mode

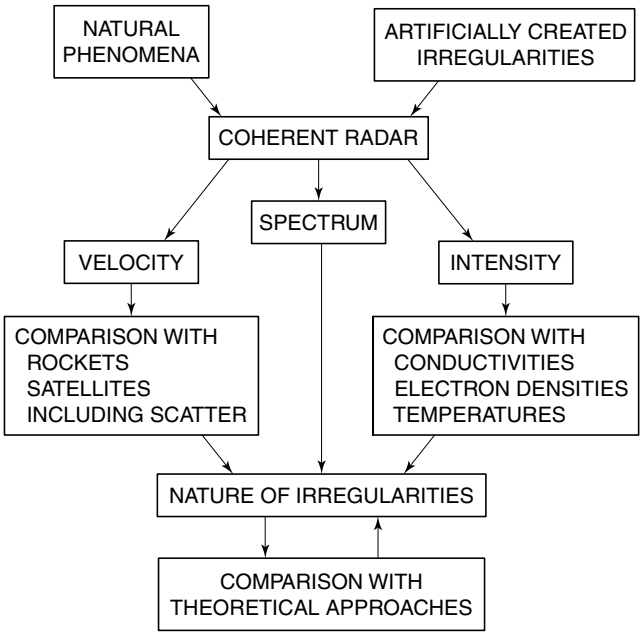

Figure 4.7. A summary of coherent-scatter radar investigations from a plasma-physics point of view (after Schlegel, 1984).

involving *direct backscatter* from FAIs, which may be significantly influenced by ionospheric refraction (depending on the frequency of the sounder). Figure 4.7 summarizes the type of information from an OBS which may be of interest to plasma physicists.

Types of oblique sounders currently in use

Having generically described the sounders in the previous section, we will proceed to classify and describe them by their operating frequency and describe several of the systems currently deployed globally. The lowest-frequency OBS systems are the VLF sounders described by Kossey *et al.* (1983), sweeping between 5 and 30 kHz using pulse widths $<$100 ms. Figure 4.8 illustrates the basic system configuration and Figure 4.9 shows data obtained during disturbed periods in the polar lower ionosphere.

To the best of the authors' knowledge, no VLF sounders are at present in operation. However, VLF sounding remains a practical technique for probing the D and E regions of the ionosphere in some detail, especially at high latitudes.

In the HF region (3–30 MHz) of the radio spectrum, the OBS technique has been employed since the mid-1920s. See Hunsucker (1991, Chapter 4) for a description of the history and theory for OBS systems. Perhaps the best examples of the HF OBS technique is the SuperDARN (Dual Auroral Radar Network) system (Greenwald *et al.*, 1995) and the PACE (Polar and Conjugate Network) system (Baker *et al.*, 1989). These HF radars operate in the frequency range of

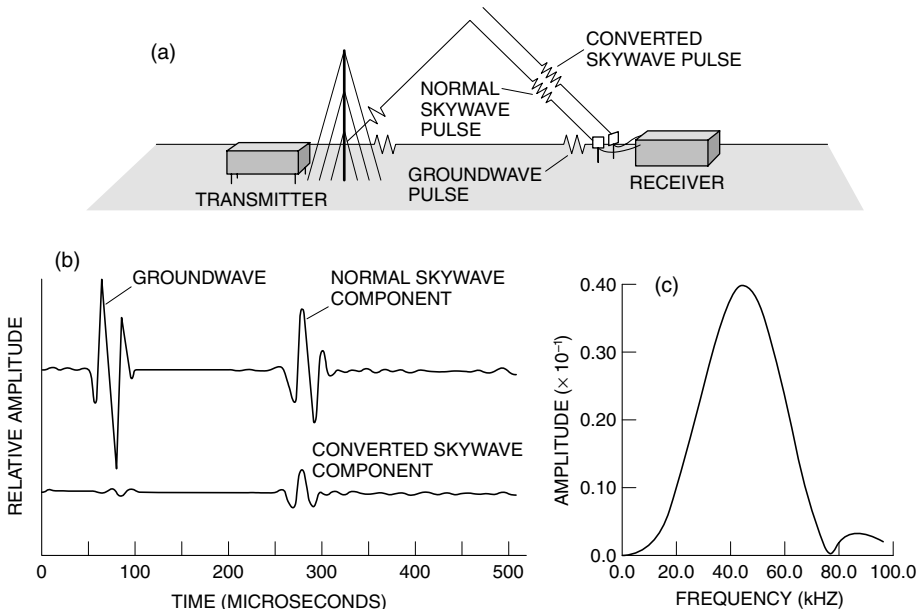

Figure 4.8. (a) The VLF pulsed-ionosonde technique. (b) An example of typical observed waveforms. (c) The spectrum of a typical transmitted pulse. (After Kossey *et al.*, 1983.)

~8–20 MHz with an azimuth coverage of 52° and extend in range from a few hundred kilometers to more than 3000 km. Backscatter from F-region ionospheric irregularities is typically observed from ~10% to 60% of this range interval. The first HF radar of this type is located in Goose Bay, Labrador (Greenwald *et al.*, 1985) and has been in continuous operation since 1983.

The present SuperDARN system covers over most of the northern polar ionosphere and part of the south polar ionosphere. The fields of view of the existing, funded, and proposed northern-hemisphere SuperDARN radars are shown in Figure 4.10 (and listed in Table 4.2) and the southern-hemisphere HF radar coverage is shown in Figure 4.11.

The SuperDARN radars utilize ionospheric refraction to achieve orthogonality with the magnetic-field-aligned irregularities in the high-latitude F region, and their frequency range of ~8–20 MHz permits achieving orthogonality over a factor of more than six in electron density. They are also frequency-agile, permitting observations at two or more different frequencies to be interwoven. An example of a SuperDARN-derived polar plasma-convection pattern is shown in Figure 4.12. The SuperDARN antenna array consists of 16 log-periodic antennas (LPAs) in the primary array and four LPAs to form a small-scale interferometer array for elevation-angle determination, as shown in Figure 4.13.

RF signals from or to these antennas are phased with electronically controlled time-delay phasing elements that allow the beam to be steered into 16 directions covering the 52° azimuth sector. The azimuthal resolution of the measurements is

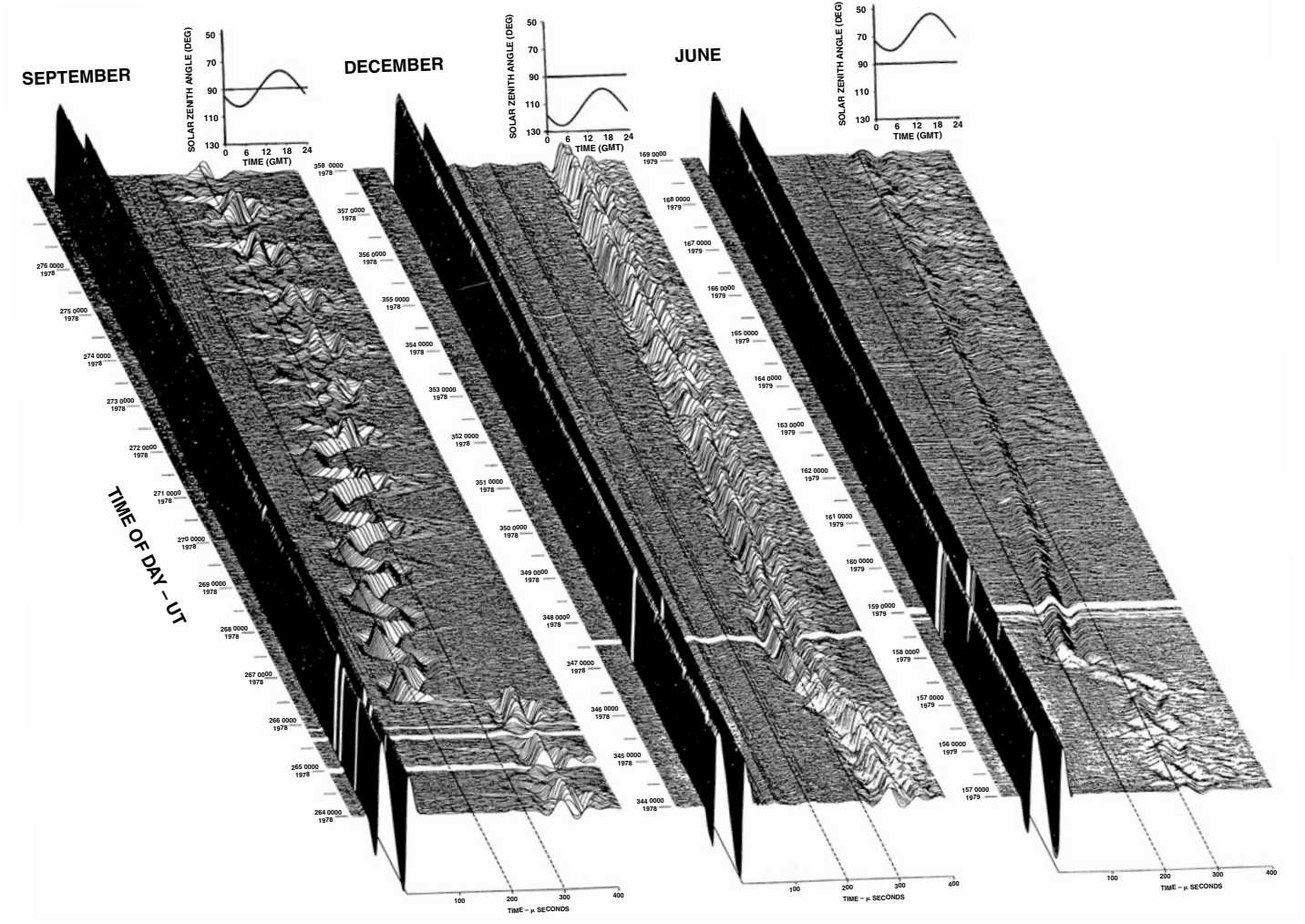

Figure 4.9. VLF pulse-reflection data for a disturbed polar period (after Kossey *et al.*, 1983).

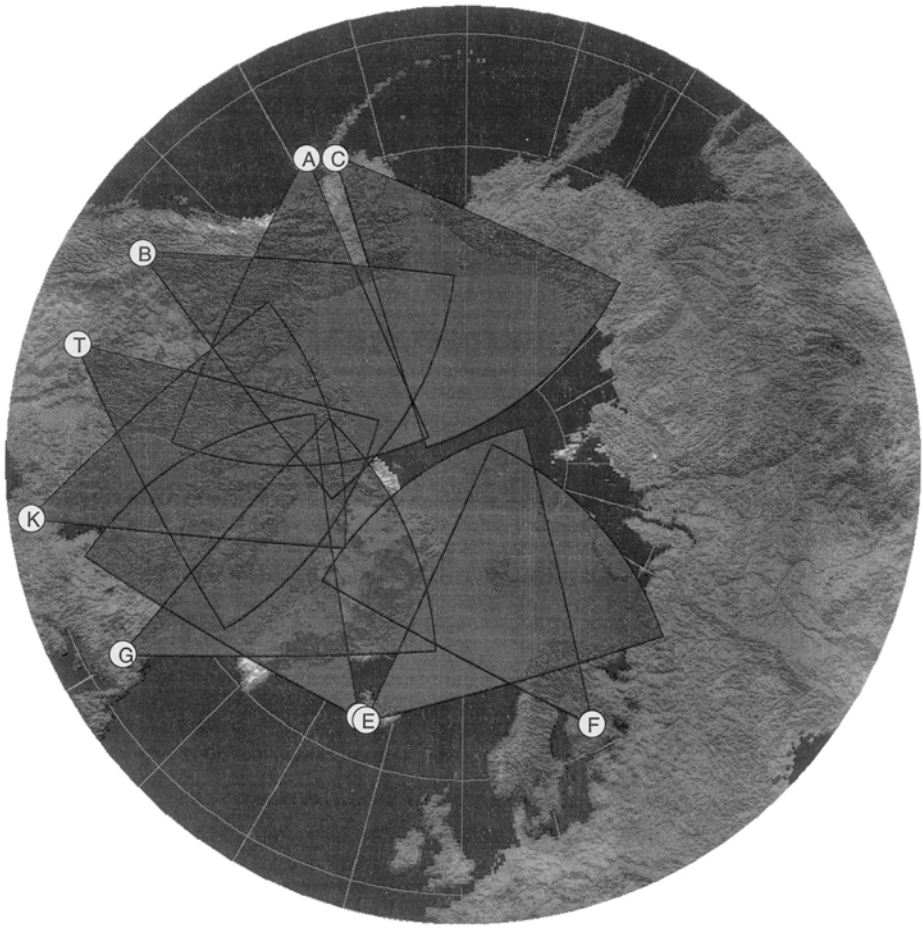

Figure 4.10 Locations and fields of view of the eight operating northern-hemisphere SuperDARN HF radars, as well as the STARE radar in northern Scandinavia and the remaining SABRE radar in Wick, Scotland (after Greenwald *et al.*, King Salmon (C), operated by the Communications Research Laboratory in Japan; Kodiak (A), operated by the Geophysical Institute UAF in the USA; Prince George (B), operated by the University of Saskatchewan in Canada; Saskatoon (T), operated by the University of Saskatchewan in Canada; Kapuskasing (K), operated by the JHU/APL in the USA; Goose Bay (G), operated by the JHU/APL in the USA; Stokkseyri (W), operated by the CNRS/LPCE in France; Þykkvibær (E), operated by the Radio and Space Plasma Physics Group, University of Leicester in the UK (also known as Cutlass/Iceland); and Hankasalmi (F), operated by the Radio and Space Plasma Physics Group, University of Leicester in the UK (also known as Cutlass/Finland).

Table 4.2. *SuperDARN radars operating in the northern hemisphere*

Radar	ID	Location	Affiliation	Latitude (°N)	Longitude (°E)	Operational
CUTLASS[a]/Finland	F	Hankasalmi, Finland	University of Leicester	62.32	26.61	April 1995
CUTLASS[a]/Iceland	E	Pykkvibær, Iceland	University of Leicester	63.77	−20.54	December 1995
Iceland West	W	Stokkseyri, Iceland	CNRS[b]	63.86	−20.02	October 1994
Goose Bay	G	Labrador, Canada	JHU/APL[c]	53.32	−60.46	June 1983
Kapuskasing	K	Ontario, Canada	JHU/APL[c]	49.39	−83.32	September 1993
Saskatoon	T	Saskatchewan, Canada	University of Saskatoon	52.16	−106.53	September 1993
Prince George	B	British Columbia, Canada	University of Saskatoon	53.98	−122.59	March 2000
Kodiak	A	Kodiak Island, Alsaska	UAF[d]	57.62	−152.19	January 2000

Notes:

[a] Co-operative United Kingdom Twin Located Auroral Sounding System.

[b] Centre National de la Recherche Scientifique.

[c] Johns Hopkins University Applied Physics Labratory.

[d] University of Alaska, Fairbanks.

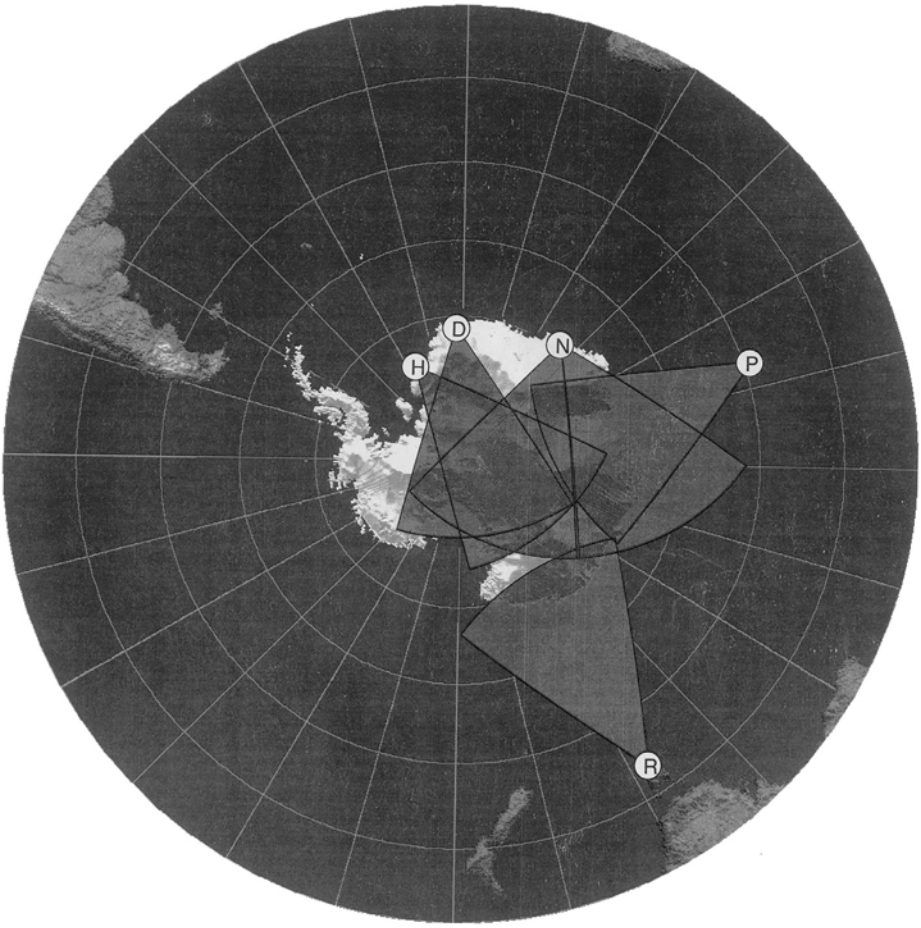

Figure 4.11. Fields of view of southern-hemisphere SuperDARN HF radars (after Greenwald *et al.*, 1995). Halley (H), operated by the British Antarctic Survey in the UK (also known as the Southern Hemisphere Auroral Radar Experiment (SHARE)); SANAE (D), operated jointly by the University of Natal and the PUCHE in the Republic of South Africa; Syowa South (J), operated by the National Institute of Polar Research in Japan; Syowa East (N), operated by the National Institute of Polar Research in Japan; Kerguelen (P), operated by the CNRS/LPCE in France; and TIGER (R), operated by the La Trobe University in Australia.

dependent on radar operating frequency and ranges from ~2.5° at 20 MHz to 6° at 8 MHz. Since most of the observations are made in the frequency range 12–14 MHz, the nominal azimuthal resolution of the radar is ~4°. At a range of 1500 km, this corresponds to a transverse spatial dimension of ~100 km.

A secondary parallel antenna array of four LPAs located 100 m in front of the primary array is used to determine the vertical angle of arrival of the backscattered signal. This secondary array also uses a phasing matrix and functions as an interferometer to determine the relative phases of the backscattered signals arriving at the two arrays. The phase information is converted into an elevation angle,

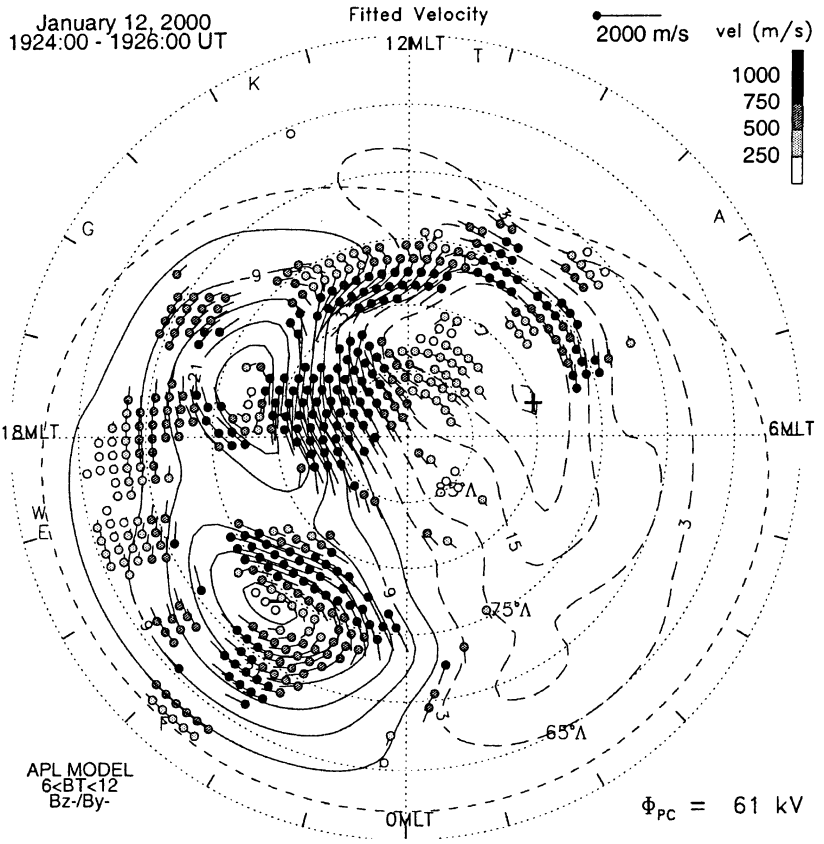

Figure 4.12. A typical polar plasma-convection pattern (courtesy of R. Greenwald).

which is used to determine the propagation modes of the backscattered signal as a function of range, as well as the approximate height of the scatterers. This secondary antenna array is also visible in Figure 4.13. The range resolution of the SuperDARN measurements is determined by the transmitted pulse length (200–300 ms) and is equivalent to 30–45 km.

Electronic steering of the SuperDARN antenna array occurs on microsecond time scales, which allows the radar to be scanned rapidly through a number of beams or to dwell for an extended time on a single beam. Typically a radar will scan in a sequential manner with a dwell time of 6 s in each beam and a full-scan time of 96 s.

Although very useful information has been obtained using single HF radars, it became apparent that bi-directional common-volume observations with radar separations greater than 500 km were the best approach to advancing the study of high-latitude convection with HF radars (Ruohoniemi *et al.*, 1989). The common field of view of a pair of HF SuperDARN antennas covers 15–20° of invariant latitude and 3 h of magnetic local time. The fields of view of several pairs of HF

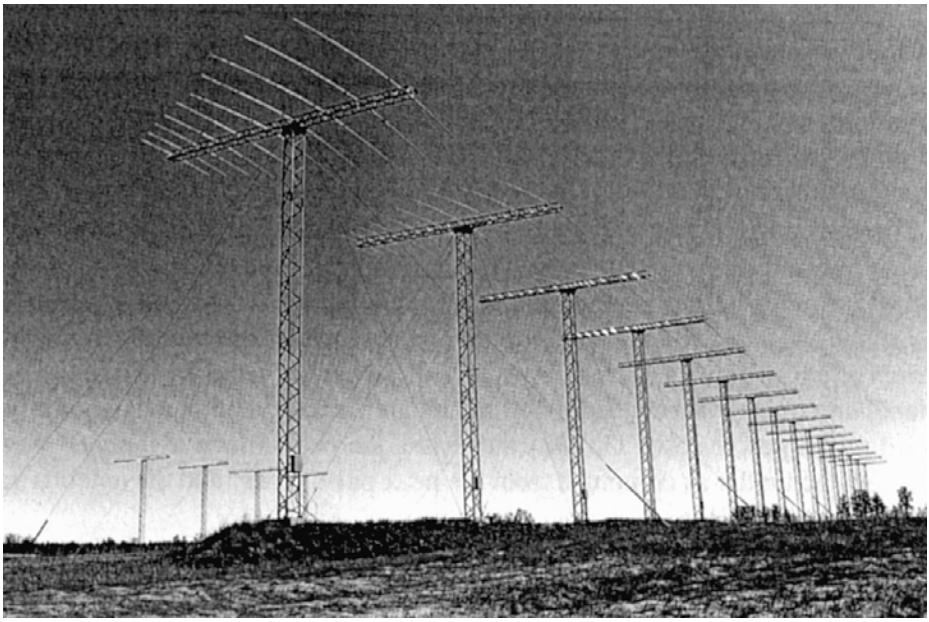

Figure 4.13. The SuperDARN HF antenna array at Kapuskasing, Ontario (after Greenwald *et al.*, 1995).

radars extend the spatial coverage of the high-latitude auroral zone and the polar-cap boundary over many hours of magnetic local time. If ionospheric irregularities were to fill this common viewing area, it would be possible to monitor the dynamics of plasma convection over a significant part of a convection cell. The rates of occurrence of HF scattering during a solar-cycle maximum are given by Ruohoniemi and Greenwald (1997).

Figure 4.14 is a sketch of the manner in which VHF and HF radars intercept field-aligned irregularities in the high-latitude E and F regions and Figure 4.15 shows a comparison between F-region Doppler velocities obtained simultaneously with the Sondrestrom ISR and the Goose Bay HF radar. More details on the SuperDARN system may be found in the review paper by Greenwald *et al.*, (1995) and on the SuperDARN homepage on the internet.

At VHF/UHF frequencies, OBS systems are primarily used as auroral radars and sometimes, at near-equatorial latitudes, to investigate irregularity structures associated with the equatorial electrojet. See Kelley (1989) for the physics of auroral and equatorial VHF/UHF echoes. Examples of VHF/UHF radars used in research into auroral and equatorial ionospheric irregularities are the Cornell University Portable Interferometer (CUPRI) (Providakes, 1985), the Saskatchewan Auroral Polarimetric Phased Ionospheric Radar Experiment (SAPPHIRE), (Kustov *et al.*, 1996 and (1997). Auroral radars are exemplified by the Scandinavian Twin Auroral Radar Experiment (STARE), which was first described by Greenwald *et al.*, (1978). The STARE system consists of two pulsed

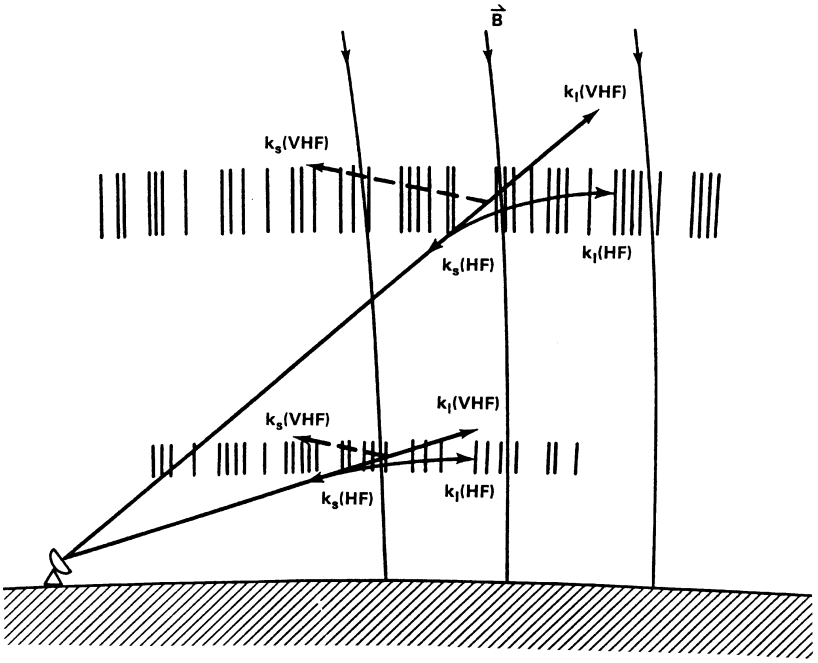

Figure 4.14. Idealized ray paths for VHF and HF radars to E-region and F-region FAIs (after Greenwald *et al.*, 1995).

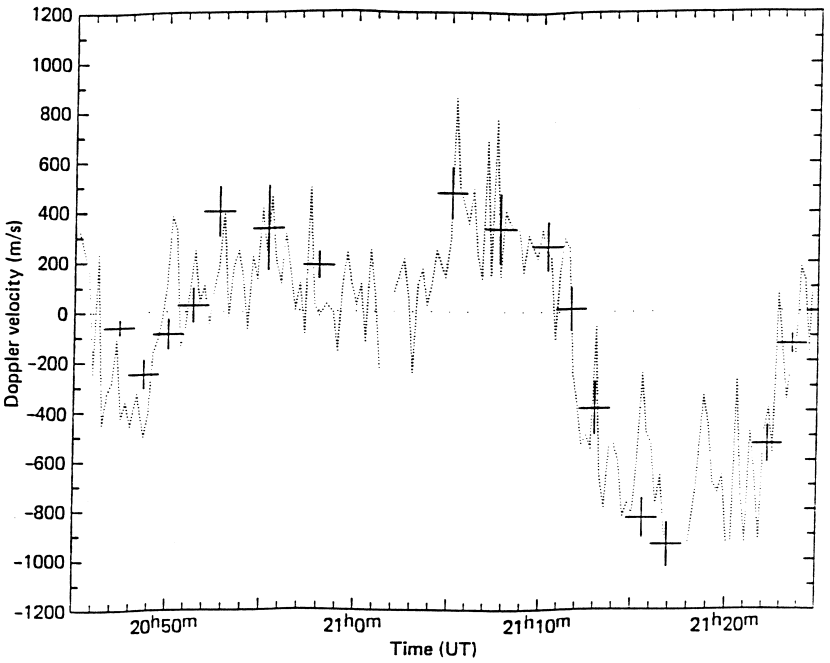

Figure 4.15. A comparison of F-region Doppler velocities obtained with the Goose Bay HF radar and velocities obtained by the Sondrestrom ISR (after Greenwald *et al.*, 1995).

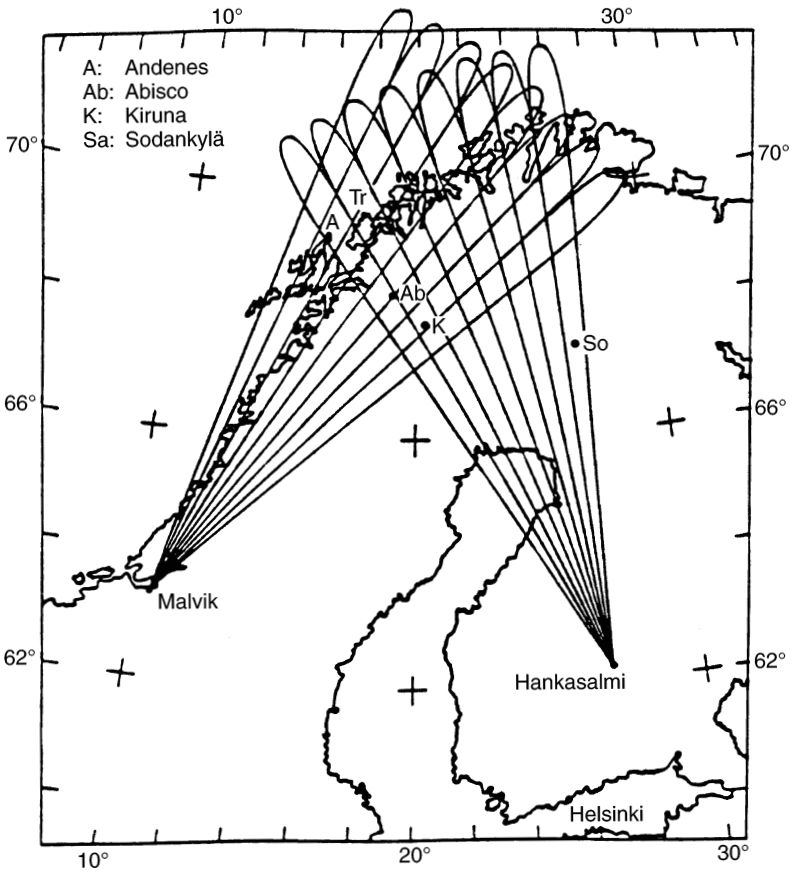

Figure 4.16. A map of the eight overlapping beams of the STARE radar over northern Scandinavia (after Greenwald *et al.*, 1978).

bistatic phased-array radars located at Malvik, Norway and Hankasalmi, Finland. Beams from the radars are directed over a large common-viewing area (approximately 16000 km^2) centered on the auroral zone in northern Scandinavia – as illustrated in Figure 4.16.

The Doppler data from the two radars are combined to determine the vector velocity of the irregularities with 20-km × 20-km spatial and 20-s temporal resolution. An example of the data obtained with the STARE system and simultaneous all-sky-camera data is shown in Figure 4.17 illustrating a westward-traveling auroral surge. (See Section 6.4.) A list of OBSs (coherent radars) deployed globally as of 2000 is shown in Table 4.3.

Some of the advanced OBS systems employ arrays of interferometer antennas (Farley *et al.*, 1981) similar to those used in radio astronomy. The Fourier transform of the digitized signals from the respective antennas is taken, and the complex cross-correlation spectrum for each pair is determined in the time domain. Spaced-antenna analysis can also be carried out in the frequency domain

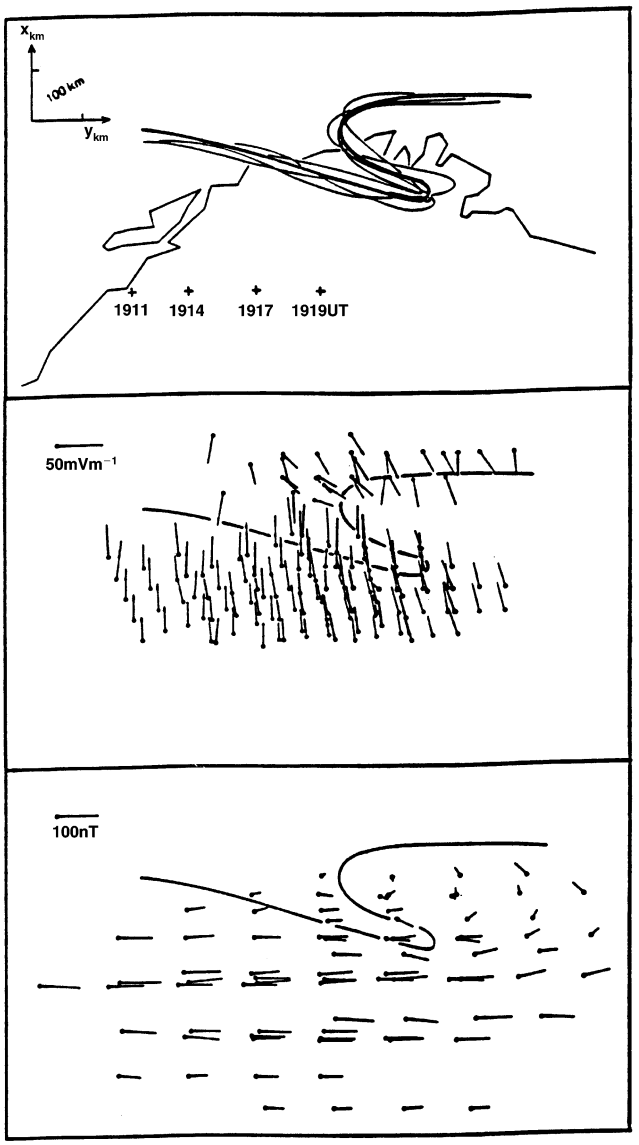

Figure 4.17. Superimposed epoch analysis of the spatial distribution of auroral luminosity (upper panel) and equivalent currents (lower panel) during the passage of a westward traveling surge at approximately 1911 UT on 27 March 1977 (from Inhester *et al.*, 1981).

(Briggs and Vincent, 1992), offering some advantages over time-domain analysis.

Two new novel approaches in the design of OBS systems are the Frequency-Agile Radar (FAR) (Tsunoda *et al.*, 1995) and the multi-use system described by Ganguli *et al.* (1999), which may be used in modes other than as an OBS, and the Manatash Ridge Radar (a passive bistatic radar for upper-atmospheric radio science) (Sahr and Lind, 1997), which utilizes transmissions from standard FM broadcast stations.

Table 4.3. *Currently deployed OBS (HF/VHF/UHF) systems*

	Radar		
Location	Name	Type	Reference/description
Finland	COSCAT/XMTR[a]	Auroral/pulsed/bistatic	McCrea *et al.* (1991); 929.5 MHz
Finland and Sweden	COSCAT/RCVRS[a]	Bistatic/pulsed and CW	0.5 kW, 4° elevation, 2° azimuth
U. K. and Sweden	SABRE	Auroral/pulsed	Jones *et al.* (1981); 150 MHz; twin radars
Scandinavia	STARE	Auroral/pulsed/bistatic	Greenwald (1987)
Canadian Arctic	SAPPHIRE[a]	Auroral and polar cap/ CW/bistatic	Kustov *et al.* (1996); 50 kW
NE Canada	SHERPA	Auroral and polar/pulsed	Hanuise *et al.* (1992)
Polar	SUPERDARN	Polar cap and auroral/ pulsed	Greenwald *et al.* (1995); 6–16 MHz; 1 kW each into 16 antennas, 52° azimuth sector
Crete	SESCAT	Mid-latitude, E region/ CW/bistatic	Haldoupis and Schlegel (1993); 50.52 MHz, 1 kW, four Yagi arrays
(Portable)	CUPRI	E region/monostatic	Providakes *et al.* (1985); 49.92 MHz, 25 kW, five antennas
(Portable)	FAR	D, E, and F regions/ pulsed	Tsunoda (1992); 2–50 MHz, various pulse widths
Halley Bay, Antarctica	PACE	Polar cap F region/pulsed	Baker *et al.* (1989); 8–20 MHz, 1 kW each into 16 antennas, 52° azimuth sector
Antarctica	SYOWA	Auroral/pulsed	50 and 112 MHz, 15 kW, 3–14-element coaxial antennas
Peru	Jicamarca	Equatorial/pulsed/ monostatic	Kelley (1989, Chapter 4); 50 MHz (oblique and vertical incidence), 49.9 MHz

Table 4.3. (*cont.*)

	Radar		
Location	Name	Type	Reference/description
Kwajalein	Altair	Equatorial/monostatic/ pulsed	Tsunoda (1981); 155.5 MHz
Japan	MU Radar	mid-latitude, monostatic/ pulsed	Kato *et al.* (1989); 46.5 MHz

Notes:
Acronyms for radars: COSCAT: Coherent scatter, CUPRI: Cornell University Portable Radar Interferometer, CW: Continuous Wave, PACE: Polar Anglo-American Conjugate Experiment, SABRE: Scandinavian and British Radar Experiment, SAPPHIRE: Saskatchewan Auroral
Polarimetric Phased Array
Ionospheric Radio Experiment, SESCAT: Sporadic-E scatter, SHERPA: System HF d'Etude Radar Polaires Auroral, STARE: Scandinavian Twin Radar Experiment, DARN: originally was Dual Auroral Radar
Network – now SUPERDARN refers to the network of HF backscatter sounders that mainly probes the polar F region, FAR: Frequency Agile Radar.
The SABRE radar in Sweden has been decommissioned, but the radar in Wick, Scotland, is still operational.

Some advantages and disadvantages of auroral and HF radars

Auroral radars

The radio ray path from these radars must intercept the Earth's magnetic field at near-normal incidence, so siting of the radars is of critical importance. This requires that transmitters and receivers be located at high-latitude sites, which are sometimes rather inhospitable and distant from "civilization," which, in turn, complicates the logistics. Also, in order to achieve the narrow azimuthal beam-widths required, rather large antenna arrays are required, affecting the cost.

HF radars

HF radar systems require larger areas for the antenna array than do VHF/UHF systems. Siting of the radars, although it is not as critical as it is for auroral radars, is important. In order to cover the entire polar cap (as in the SuperDARN system), considerable international cooperation is required. Because of their remote location, some of the sites are quite expensive to maintain. During severe auroral or polar-cap absorption the lower HF frequencies used may be unusable.

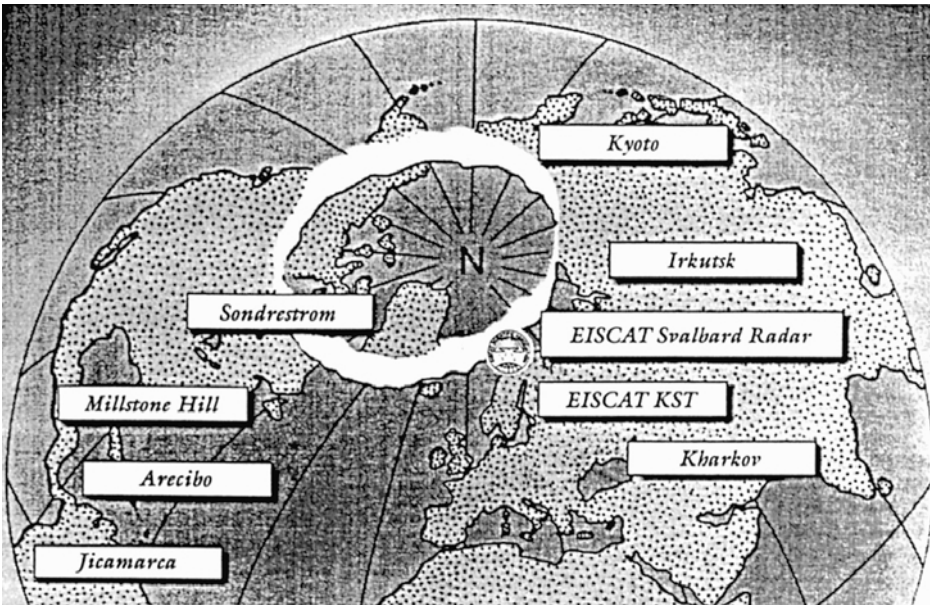

Figure 4.18. A map showing currently operational ISRs (courtesy of EISCAT Association).

4.2.3 Incoherent-scatter radars

Incoherent-scatter radars (ISRs) are a relatively new development compared with coherent backscatter techniques – they were first developed and deployed during the early 1960s. The fundamentals of the theory of incoherent scatter from the ionosphere are covered by Evans (1969), in Section 4.7 of Davies (1990), in Section 2.3.2 of Hunsucker (1991) and in Section 3.5.3 of this book. ISR technique has matured and proven to be one of the most powerful Earth-based radio techniques for probing the ionosphere and thermosphere and even for probing into the mesosphere under certain conditions. At present there are nine functional ISRs (some operating only sporadically), as shown in Figure 4.18.

Most of the ISRs in use today have been described in some detail in Chapter 7 of Hunsucker (1991) and in Section 5 of Hunsucker (1993). The newest addition to the global array of ISRs is the Longyearbyen, Svalbard installation (Figure 4.19) – which is part of the EISCAT system, whose parameters are listed in Table 4.4. The design features of the Svalbard ISR are described in detail by Wannberg *et al.*, (1997). The other operational ISRs are shown in Figure 4.18 and current facility addresses and contact personnel are listed in the current version of the NCAR CEDAR Data Base.

4.2.4 D-region absorption measurements

The power density (or *attenuation*) of radio waves at a distance, d, from the transmitter is reduced by geometric effects, refraction, absorption in the atmosphere,

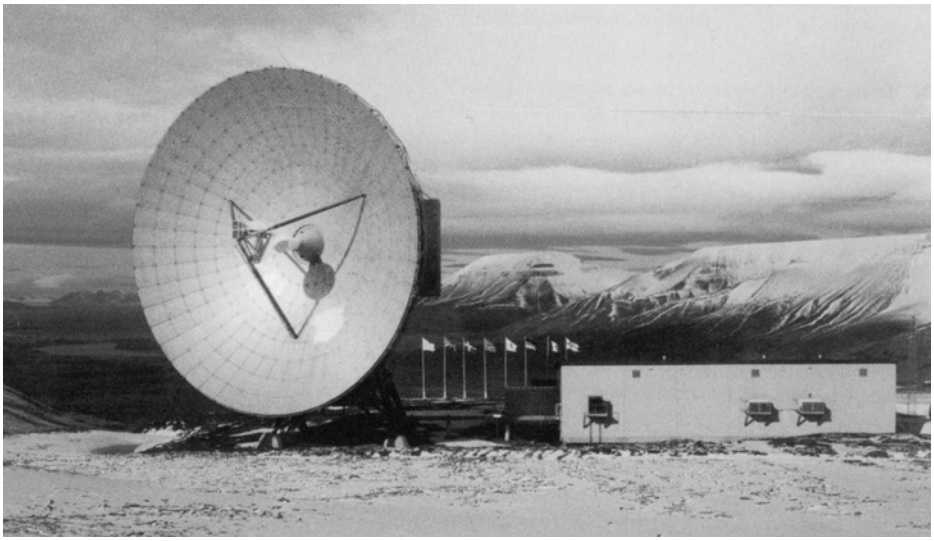

Figure 4.19. A photo of the new EISCAT ISR in Longyearbyen Svalbard (Spitzbergen) (courtesy of EISCAT Association).

and scattering and diffraction by objects in the ray path. For frequencies used in ionospheric techniques (ELF/UHF), most of the absorption occurs in the D region and is characterized as either *deviative* or *non-deviative* absorption. The theory of ionospheric absorption is treated in Davies (1990, pp. 65–66 and 215–217), Hunsucker (1991, pp. 50–53), Hargreaves (1992, pp. 65–66 and 71–72), and Section 3.4.1 of this book.

Current status and global deployment

Since there are several radio techniques for measuring ionospheric absorption, we employ the URSI designations for the most-used methods. See Rawer (1976), Davies (1990, pp. 217–219), and Hunsucker (1991, Chapter 7, pp. 165–183) for extensive descriptions of these techniques. Certain of these techniques are currently in use, whereas others have fallen into disuse for various reasons.

The URSI A1a and A1b methods

The URSI A1a method is usually employed at mid-latitudes, since the frequencies used (2–5 MHz) would be highly absorbed at auroral and polar latitudes. Basically, this method uses a stable, constant-output pulsed transmitter, an antenna with a uniform, vertically directed main lobe (and low sidelobes), plus a stable, sensitive receiver to analyze a signal that traverses the D region twice, being reflected by the E region. This technique requires very careful, frequent calibration of the system, plus a measurement of the E-region reflection coefficient. A variant of this method is the URSI A1b method, which uses the same basic equipment and modified equations for oblique incidence at short distances. The URSI A1a and A1b techniques were used rather extensively from the

Table 4.4. *Parameters of the EISCAT radar system (courtesy of EISCAT Corp.)*

	Location					
	Tromsø		Kiruna	Sodankylä	Longyearbyen	
Geographic coordinates	69°35′ N 19°14′ E		67°52′ N 20°26′ E	67°22′ N 26°38′ E	78°09′ N 16°02′ E	
Geomagnetic inclination	77°30′ N		76°48′ N	76°43′ N	82°06′ N	
Invariant latitude	66°12′ N		64°27′ N	63°34′ N	75°18′ N	
Band	VHF	UHF	UHF	UHF	UHF	
Frequency (MHz)	224	931	931	931	500	
Maximum bandwith (MHz)	3	8	8	8	10	
Transmitter	2 klystrons	1 klystron	–	–	16 klystrons	
Channels	8	8	8	8	6	
Peak power (MW)	2×1.5	1.3	–	–	1.0	
Average power (MW)	2×0.19	0.16	–	–	0.25	
Pulse duration (ms)	0.001–2.0	0.001–1.0	–	–	<0.001–2.0	
Phase coding	Binary	Binary	Binary	Binary	Binary	
Minimum interpulse time (ms)	1.0	1.0	–	–	0.1	
Receiver	Analog	Analog	Analog	Analog	Analog–digital	
System temperature (K)	250–350	70–80	30–35	30–35	55–65	
Digital processing	8-bit ADC, 32-bit complex, ACFs, parallel channels				12-bit ADC, Lag profiles 32-bit complex	
					Antenna 1	Antenna 2
Antenna	Cylinder 120 m×40 m	Dish 32 m	Dish 32 m	Dish 32 m	Dish 32 m	Dish 42 m fixed
Feed system	Line feed	Cassegrain	Cassegrain	Cassegrain	Cassegrain	
Cassegrain	128 crossed dipoles					
Gain (dBi)	46	48	48	48	42.5	45
Polarization	Circular	Circular	Any	Any	Circular	Circular

Note:
ACFs, autocorrelation functions

mid-1950s through the mid-1970s, but, to the best of the authors' knowledge, only a few installations are still in operation. However, it remains a useful method – especially in view of advances in VLSI, DSP, antenna theory, and computer techniques.

The URSI A2 method

Brief discussions of the URSI A2 cosmic-noise method of measuring absorption may be found in Davies (1990, pp. 218–219 and in Hargreaves (1992, pp. 71–72), and a rather extended discussion in Hunsucker (1991, pp. 169–178). The instrument used to make URSI A2 absorption measurements is called the *riometer* (Relative Ionospheric Opacity Meter, Extra-terrestrial Electromagnetic Radiation). It was designed and built at the Geophysical Institute of the University of Alaska (Little and Leinbach, 1959), and was first globally deployed during the International Geophysical Year (IGY), 1957–1959. It was based on work done in the early 1950s by several investigators, and the riometer was found to be ideally suited for measuring the strong D-region absorption at high latitudes. Indeed, both polar-cap and auroral-zone absorption were verified using this instrument. See also Hargreaves (1969).

In essence the riometer is just a stable radio receiver, and, in its usual form, this stability is achieved by switching the receiver input rapidly between the signal and a stable local noise source, a principle first enunciated by Machin *et al.* (1952). The riometer operates at some frequency above the penetration frequency of the ionosphere so that it receives the signal coming from outer space – i.e. the cosmic-radio noise. Since the intensity of the cosmic noise source does not vary, reductions of the received intensity are interpreted to mean that the signal has been absorbed somewhere in the ionosphere.

The cosmic-noise absorption in decibels can be calculated by using

$$A = 10\log_{10}(P_0/P), \tag{4.1}$$

where P_0 is the power output in the absence of the ionosphere and P is the power output of the riometer. A plot of typical riometer results is shown in Figure 4.20.

Although the cosmic noise may be assumed constant over time, it is not constant over the sky. The riometer antenna, which points in a fixed direction from the observing site – to the zenith, for example – is scanned around the radio sky as the Earth rotates, coming back to the same place every sidereal day (24 h, 4 min). In order to measure the absorption, we must know what the intensity would have been in the absence of the absorption. This is usually estimated by superimposing measurements over some period of time as a function of sidereal time, and taking a line along the top of the distribution to indicate the intensity when absorption is absent. The resulting curve is generally called the *quiet-day curve (QDC)*, and, although the idea is simple, the accurate derivation of the QDC can be the most difficult part of absorption measurement by the riometer technique (Krishnaswamy *et al.*, 1985).

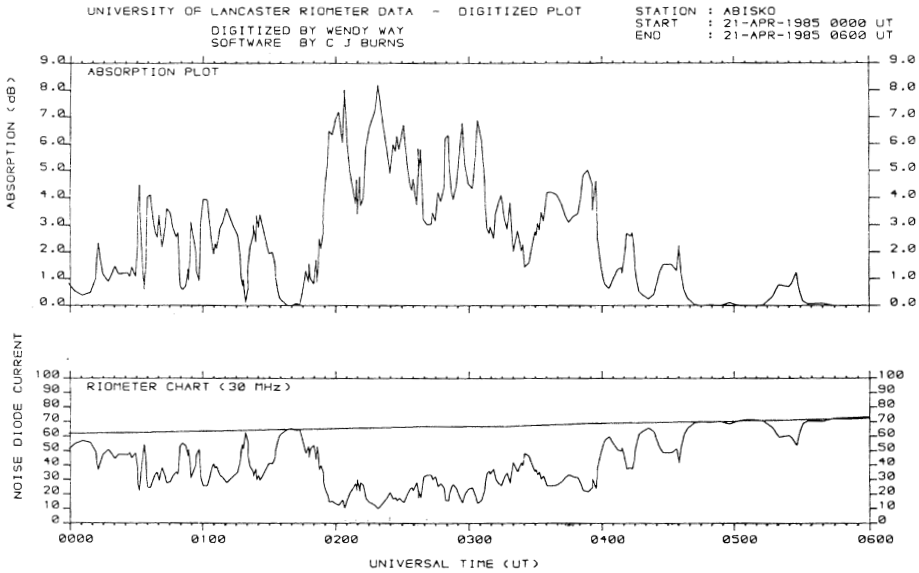

Figure 4.20. Auroral radio absorption at 30 MHz over a 6-h period. On the riometer chart (lower panel) the "noise diode current" is proportional to the received cosmic noise power, and the straight line is the 'quiet-day curve' representing the power that would be received in the absence of absorption.

Most riometers have operated with a small antenna that has a wide beam – e.g. ~60° between half-power points. This has been done for practical reasons, but it does bring a disadvantage in that the antenna pattern projects to a region about 100 km across in the D region. Therefore a standard riometer installation does not have good spatial resolution. In recent years, however, there has been an increase in narrow-beam work and in the use of imaging riometers.

The absorption depends on the radio frequency as the inverse square (see Section 3.4.1), and this is one factor that influences the choice of a frequency for the riometer. At higher VHF frequencies the antenna can be smaller (for a given beamwidth) but the instrument becomes less sensitive to weak absorption. At the lower VHF frequencies the antenna must be large and also there is more interference from ionospherically propagated signals. The compromise has generally led to using the 30–50-MHz band. When data are obtained at several frequencies, it is usual to reduce the results to 30 MHz for comparison purposes,

$$A(30\ \text{MHz}) = A(f)(30)^2/f^2 \tag{4.2}$$

The first generation of riometers (from the IGY/IGC era) used vacuum tubes, and solid-state circuits were introduced into this type of instrument in the 1960s, which permitted the riometer to be packaged as a small unit with low power comsumption. A problem with the solid-state riometer, however, was a lack of discrimination against interference in the front end, but this has been remedied using ceramic filters and integrated circuits (Chivers, 1999, personal communication).

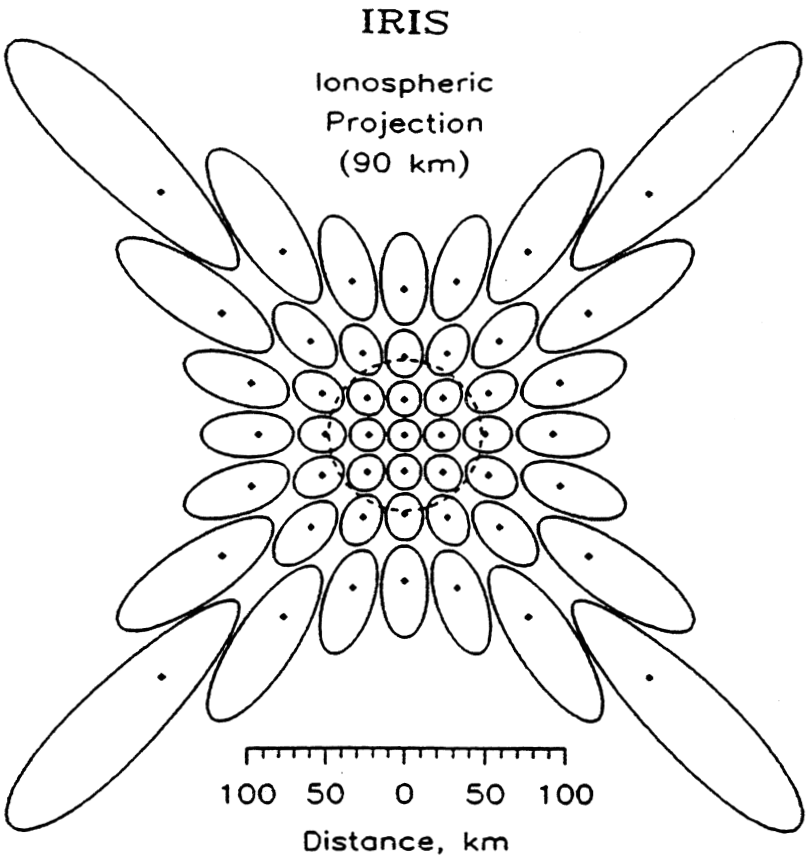

Figure 4.21. Projection of the IRIS beams at 90 km altitude (Derrick and Rosenberg, 1990). The beam centers are marked as dots, and the 3-dB levels as solid lines. The dashed circle is the projection of a typical wide-beam riometer antenna.

Imaging riometry

Technical developments have now made it possible to construct riometer systems that produce a large number of narrow beams simultaneously, sufficient to construct a picture of the absorbing region out to, say, 150 km (horizontal) from the installation. Several such systems are operating at the time of writing (2002), and several more are planned. These systems are called *imaging riometers.*

The first Imaging Riometer for Ionospheric Studies (IRIS) was installed at the South Pole in 1988–1989 (Detrick and Rosenberg, 1990). It forms 49 beams and the best resolution is about 29 km at the 90-km level (Figure 4.21).

In principle, one could use 49 riometers to record the signals, but, to reduce the number, this system switches the signals sequentially among seven riometers; and, although this implies some loss of sensitivity, it is nevertheless adequate for observations at a time resolution of 10 s. The operating frequency is 38.2 MHz.

The imaging riometers have demonstrated that the absorption contains features of finer scale, whose motions may be also be observed. This type of system

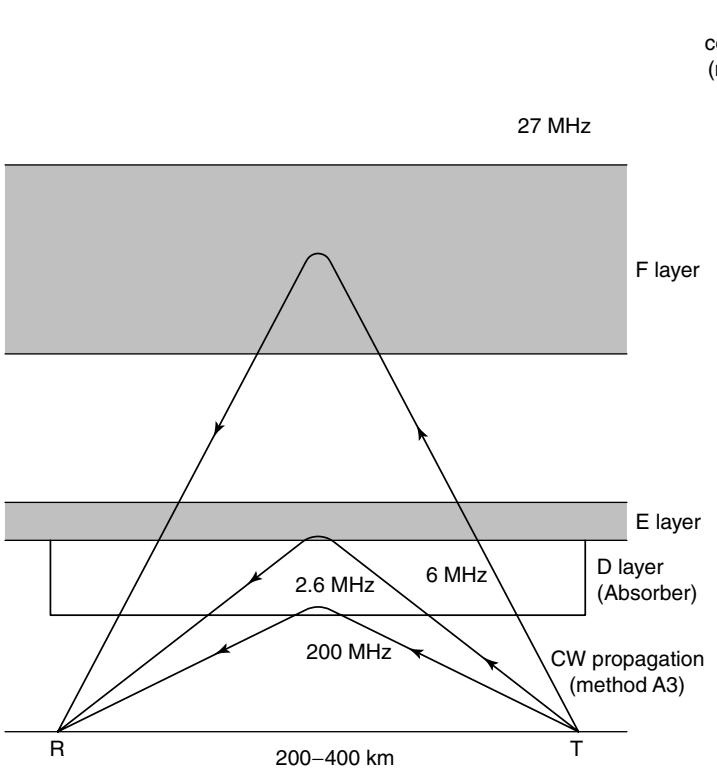

Figure 4.22. The geometry for the A3 absorption-measurement method. The dashed line from R to the Pole Star is an idealized ray path for the A2 (riometer) method (after Rawer, 1976).

is expected to produce a lot of new information about the structure and dynamics of auroral radio absorption, and the occurrence of finer-scale absorption must have implications for the effect of auroral absorption on HF radio propagation related to high-resolution systems. Some results are given in Sections 7.2.2 and 7.2.4.

URSI A3a and A3b methods

The URSI A3 technique uses short, one-hop ionospheric modes at LF through HF frequencies at mid-latitudes, and the basic geometry is shown in Figure 4.22. The A3a method consists of CW field-strength measurements at oblique incidence over ground distances of 200–400 km, using frequencies from 2–3 and 6 MHz. The vertical-plane antenna patterns must be very uniform, so that small changes in reflecting-layer height will not affect the system losses, and one dominant mode must be used. Transmitter outputs and receiver sensitivities must be stable and calibrated, and no significant groundwave should be present to contaminate the results. This method is probably most applicable for long-term measurement of seasonal and sunspot variations of D-region absorption at mid-latitudes.

The main difference with the URSI A3b mode is that it uses frequencies in and

below the MF band, where the groundwave is quite strong. Therefore, a vertical-loop antenna, with its plane perpendicular to the direction of the transmitter, is used to null out the groundwave, and another antenna is used to receive the skywave. The URSI A3a and A3b methods are described in considerable detail in the *URSI Handbook*, by Rawer (1976).

Gardner and Pawsey (1953) and Belrose and Burke (1964) pioneered the development of the partial-reflection-experiment (PRE) technique. This involves a high-powered transmitter and a sensitive receiver, operating at frequencies not near the plasma frequency. The receiving antenna array has vertically directed lobes, which can distinguish between the downcoming x and o polarizations. So, by measuring the amplitudes of both magnetoionic components, one may obtain information on the D-region electron density, collision frequency, and absorption. The PRE technique has been further enhanced by measuring both the amplitude and the phase of the downcoming waves. This is a differential-phase measurement. Belrose (1970) and Meek and Manson (1987) have used MF radars in the *interferometric* mode to obtain more information on the middle atmosphere and the lower D region. PRE theory and experimental results were outlined in Hargreaves (1992, pp. 28–29 and 76–77) and in Hunsucker (1991, pp. 180–182). Other techniques that have been used to measure D-region absorption are described in Hunsucker (1991, pp. 182–183) and in Hunsucker (1993, pp. 459–464). Table 4.5 summarizes most of the absorption-measurement techniques.

4.2.5 Ionospheric modification by HF transmitters

During the early years of radio broadcasting Butt (1933) and Tellegin (1933) published papers describing observations of the transfer of modulation from one transmitted signal to another signal, and Tellegen correctly described the phenomenon as radio-wave interaction in the ionosphere. This was labeled in following publications as the "Luxembourg effect" (or the "Luxembourg–Gorkii effect"). Bailey (1937) was apparently the first to suggest that the ionosphere could be "heated" by a powerful HF transmitter and that this heating could produce new information about the ionosphere. "Ionospheric heating" was not experimentally confirmed until the 1960s, and results were not published until 1970, by Utlaut.

Experimental and theoretical studies of "ionospheric cross-modulation," however, were pursued from the 1940s until the 1970s, when funding for this research decreased, due to the high operating and maintenance costs of these facilities and the advent of other less expensive facilities.

Davies (1990) devoted an entire chapter (pp. 506–537) to ionospheric modification, as did Hunsucker (1991, pp. 142–164). The former stressed results of modification experiments, whereas the latter stressed the technique. Another description (mainly theoretical) of ionospheric modification was Chapter 10 (pp. 267–284) by Erukhimov and Mityakov in the *WITS Handbook* (Liu, 1989). Radio-wave interaction and ionospheric heating were also discussed by Hargreaves (1992, pp. 93–94).

Basic principles

It is possible to modify the ionosphere by heating it with a high-powered HF transmitter, releasing chemicals, using plasma-beam injection, explosions, and tropospheric (severe weather – Davies (1990, pp. 507–511)) and VLF wave injection. We will restrict our discussion to HF waves interacting with the ionosphere.

A generic wave-interaction experiment is described in Figure 4.23 and the accompanying caption. Similarly, a generic HF heating experiment is described schematically in Figure 4.24 and the stages of the heating process are shown in Figure 4.25.

An outline of cross-modulation theory was given by Hunsucker (1991, pp. 146–152); HF heating theory was given on pp. 152–155; and also by Erukhimov and Mityakov in the *WITS Handbook* (Liu, 1989). Some special theoretical considerations, which apply to HF heating of the high-latitude ionosphere, were

Table 4.5. *Capabilities and limitations of absorption-measurement techniques*

URSI designation or other name	Capabilities	Limitations	Remarks
A1 method	Quite sensitive	Interference, cannot measure high values	For mid- or low latitudes
A2 method	Large dynamic range	Not as sensitive as some other methods	Passive, low cost, can be used to measure polar-cap and auroral absorption
A3a method	Quite sensitive	Interference, more complex than A1	Mid- or low latitude
A3b method	Sensitive	Interference	Mid- or low latitude
PRE method	Can obtain electron and collision-frequency profiles	Interference, complex system, more expensive than others	MF radar can be used to probe the middle atmosphere
$f_{\min}$ method	Can give a qualitative indication of variation of absorption	Very sensitive to variations in equipment parameters	Really not too useful
LOF	Gives a value that can be applied fairly directly to HF circuits	Interference, difficult to interpret	Not used very much
Satellite HF beacon	Global coverage	Too many variables	Not too useful

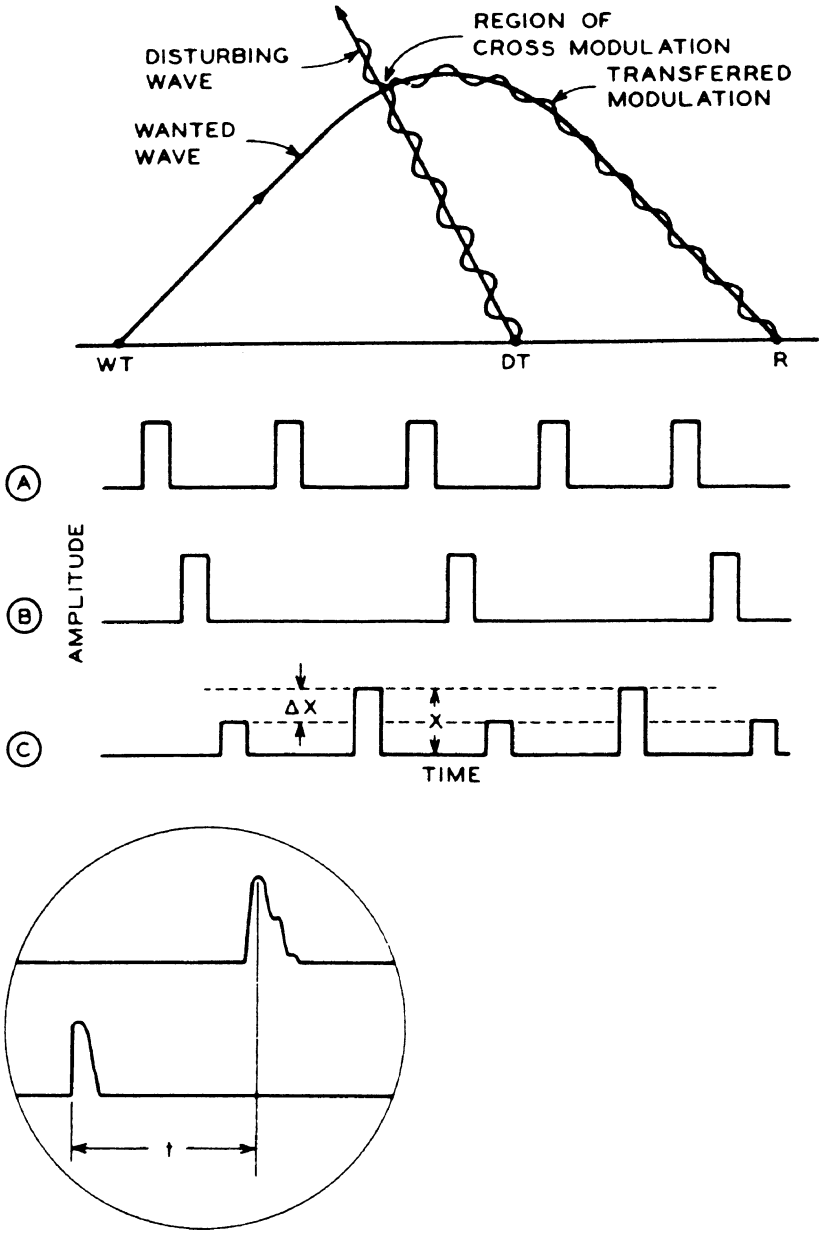

Figure 4.23. The geometry and nomenclature describing a generic ionospheric cross-modulation experiment (from Hunsucker, 1991). WT, "wanted" transmitter; DT, "disturbing" transmitter; R, receiver; A, WT keying sequence; B, DT keying sequence; C, detected echo amplitude of the wanted wave (for 50% cross modulation) at the receiver. The bottom panel shows the technique for measuring the height of attenuation. The upper trace is the received wanted echo; the lower trace is the DT pulse.

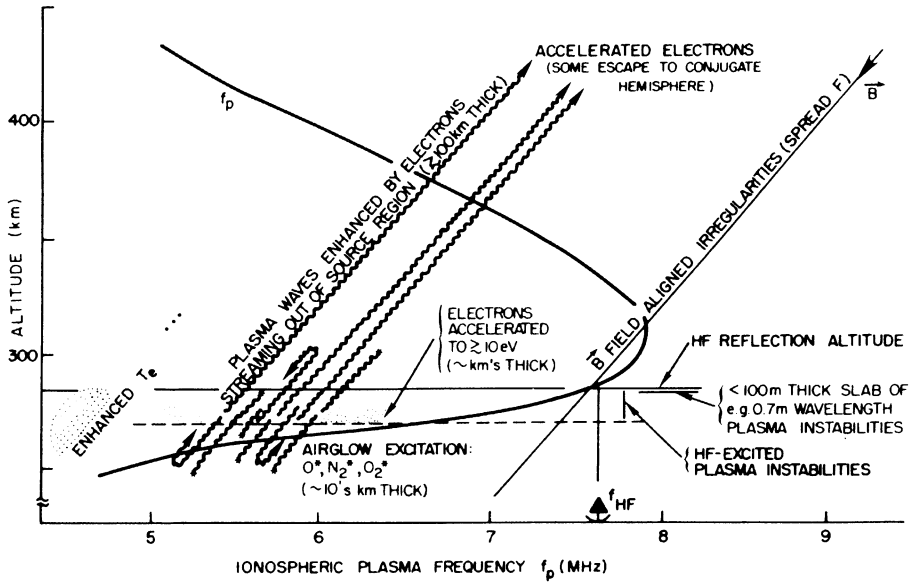

Figure 4.24. Some of the effects produced by high-power HF heating facilities (after Carlson and Duncan, 1977).

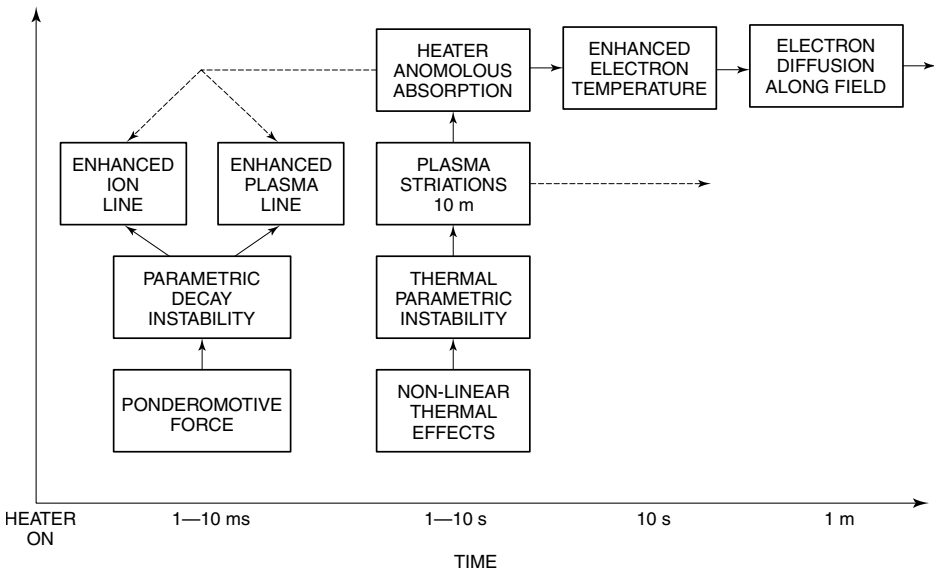

Figure 4.25. A schematic representation of the four stages of ionospheric heating (from Jones *et al.* 1986).

presented by Stubbe *et al.* (1985), in a special edition of *Radio Science,* edited by Wong *et al.* (Wong, 1990). Table 4.6 lists the ionospheric modification facilities in operation from c. 1970 to the present time.

Capabilities and limitations of ionospheric-modification techniques

The HF stimulation of the ionospheric plasma produces both linear and non-linear effects, and a wide spectrum of scale sizes and lifetimes of irregularities, as well as modulating ionospheric-current systems to produce VLF and ELF propagation. This has proven to be an extremely important technique, stimulating many experimental and theoretical advances (see Carlson and Duncan, 1977; Hunsucker, 1991, pp. 162–163, and the *Proceedings of the AGARD Conference on Ionospheric Modification*, 1991.) It has also been demonstrated that the auroral electrojet can be modified by HF-modulated stimulation, to produce both VLF

Table 4.6. *Ionospheric-modification facilities in operation since 1970*

HF heaters and their locations	Parameters	Remarks and references
NAIC; Arecibo, Puerto Rico, USA	18° N/67° W; 300 MW/3–15 MHz	Operational in 1971; Gordon *et al.* (1971)
EISCAT; Tromsø, Norway	69.6° N; 1200 MW	
HIPAS UCLA, USA	64.9° N/146.9° W; 50 MW/2.8–4.9 MHz	Wong *et al.* (1983)
Established by the USSR Gissar (Dushanbe)	38° N; 6–8 MW/4–6 MHz	Operational in 1981 Erukhimov *et al.* (1985)
Khar'kov	50° N; 6–12 MHz	Bogdan *et al.* (1980)
Moscow	56° N; 1000 MW/1.35 MHz	Schluyger (1974)
Sura Radiophysics Research Institute Nizhni Novgorod	56° N; 4.5–9 MHz	Belov *et al.* (1981)
Zimenki	56° N; 20 MW/ 4.6–5.7 MHz	Getmatsey *et al.* (1973)
Monchegorsk	68° N; 10 MW/3.3 MHz	Kaputsin *et al.* (1977)
HAARP, Alaska, USA	63° N; 145.1° W; 2.8–10 MHz	www.haarp.alaska.edu

Notes:
1. Several diagnostic techniques are usually employed at the HF heater sites to detect ionospheric changes caused by the heater. Some typical diagnostics include ISRs, ionosondes, coherent radars, and spectro-photometers.
2. The description of the facilities in this table incorporates the latest information available to the author at the time of writing.

and ELF radiation. This technique is quite expensive, both in terms of initial costs and in terms of operating and maintenance costs, which means that most operations are in the *campaign* mode. Also, because of the high levels of effective radiated power and the large area needed for high-gain antenna arrays, environmental-impact studies can drive up the capital costs, and require special measures to reduce possibly harmful radiation effects.

4.3 Space-based systems

4.3.1 A history of Earth-satellite and radio-rocket probing

Hey *et al.* (1946) were probably the first scientists to realize that extraterrestrial sources could be utilized to study the ionosphere. Subsequently, Smith *et al.* (1950), Little (1952), and Hewish (1952) showed that the radio-star emanations could be used to study the irregular nature of the ionosphere. Radar echoes from the moon resulted in the discovery of the ionospheric Faraday-rotation effect (Murray and Hargreaves, 1954; Browne *et al.*, 1956; Evans, 1956). With the advent of the artificial-Earth-satellite era (Sputnik, October 1957), satellite radio beacons were utilized to study the ionosphere. As electronics technology and rocket-booster capabilities advanced, it became possible to actually place miniaturized ionosondes into orbit, starting with the Canadian–US Alouette I topside sounder in 1962.

Actual *in situ* measurements of the ionospheric plasma from rockets and satellites have been made since the late 1940s, and a variety of radio-frequency (RF) probes has been utilized. The Langmuir probe, retarding-potential analyzers, plasma-drift meters, etc. are not really RF devices; they have been described by Kelley (1989, pp. 437–454), but will not be discussed in this book.

During the last decade, several books that discuss Earth-satellite and rocket-radio techniques for probing the Earth's ionosphere have been published (Liu, 1989, pp. 44–147; Davies, 1990, pp. 260–296; Hunsucker, 1991, pp. 187–207; Hargreaves, 1992, pp. 64–65 and 67–71).

4.3.2 Basic principles of operation and current deployment of radio-beacon experiments

The first class of satellite experiments carries an onboard transmitter (a radio beacon) and utilizes a network (sometimes global in coverage) to receive the transmissions. The daily, seasonal, geographic, and magnetic-storm-time variations of the total electron content (TEC) of the ionosphere have been obtained for the global ionosphere from various radio-beacon-experiment (RBE) satellites since the early 1960s. These TEC studies have yielded information on the large-scale changes in the ionosphere, such as orders-of-magnitude changes in TEC and medium-scale variations such as those caused

by atmospheric gravity waves (AGWs). Another class of experiments measures the scintillations in phase and amplitude of a stable (usually multi-frequency) beacon transmitter, thus providing information on the fine structure of ionospheric irregularities.

The TEC can be determined from RBE satellites by measuring the differential Doppler effect between two signals (Bowhill, 1958), the Faraday rotation of the electric vector, the modulation phase (or group delay) between two different frequencies, or the carrier-phase difference between two widely spaced frequencies. Most of the TEC studies, from the early 1960s through the mid-1970s, simply monitored the transmissions of radio beacons aboard the satellite whose primary purpose was to track the satellite, and both near-polar-orbiting and geostationary satellites were used as "targets of opportunity."

The first results obtained using geostationary satellite RBEs were reported by (Garriott *et al.*, 1965). Hargreaves developed the first proposal for a geosynchronous RBE specifically designed for ionospheric studies, which was described by Davies *et al.*,1975. More recent RBE studies involve the geostationary ETS-1 and ETS-2, the US Navy NNSS (TRANSIT) satellites, and the GPS constellation. Other RBE satellites, used for studies both of TEC and of scintillation, were WIDEBAND and POLAR BEAR.

More recently, the constellation of GPS satellites has provided much new information on ionospheric morphology and the structure of irregularities from TEC and tomographic methods (Davies, 1990; Crain *et al.*, (1993). The geometry and equations describing Faraday rotation, scintillation, and other TEC methodologies are described by Fremouw *et al.* (1978), Basu *et al.* (1988), Ho *et al.* (1996), and Pi *et al.* (1997), and in Sections 3.4.4 and 3.4.5 of this book.

4.3.3 Topside sounders

As mentioned in the introductory paragraph to this section, it became possible to place miniaturized sounders in satellites in the early 1960s, thus initiating the era of continuous global monitoring of the ionosphere using topside ionosondes. Several topside sounders have been launched and have performed beyond expectations in the last three decades: Alouette I (1962), Explorer (1964), Alouette II (1965), ISIS-I (1969), Cosmos-381 (1970), ISIS-B (1964), ISS-B (1978), EXOS-B (1978), Intercosmos-19 (1979), EXOS-C (1984), Cosmos 1809 (1984) and ISEE-1 and 2 (1979). Strictly speaking, EXOS-B, EXOS-C, and ISEE-1 are not topside sounders in the ionosonde sense, but they are "relaxation sounders" used to excite plasma waves *in situ*. Again, we are fortunate to have extended descriptions in the literature: the *WITS Handbook*, edited by Liu (1989), Davies (1990, pp. 261–273), Hunsucker (1991, pp. 200–203), and Hargreaves (1992, pp. 64–65). Vast quantities of data have been obtained using topside sounders, some of which have not been analyzed. As an example, the Alouette/ISIS series of sounders provided 50 satellite years of measurements, and has led to the publication of over 1000 papers (see Jackson, 1986, and Benson, 1997).

4.3.4 *In situ* techniques for satellites and rockets

In situ RF probes used aboard rockets and satellites were described in detail in the *WITS Handbook*, by Hunsucker (1991, pp. 205–207), and by Hargreaves (1992, pp. 52–53). These methods of trans-ionospheric propagation can be adapted to investigate the lower ionosphere. Since the signal need not penetrate the denser part of the ionosphere, its frequency can be reduced to make the observations more sensitive. The electron density and collision frequency can then be determined as functions of height as the rocket ascends and descends.

One basic type of instrument is the RF impedance probe, which was first suggested by Jackson and Kane (1959)]. Its basic principle of operation is that the input impedance of an electrically short antenna is given by a capacitive reactance $(1/(\omega C_0))$ in free space, but the behavior departs from C_0 when it is immersed in a plasma.

Another basic *in situ* probe is the *resonance probe,* which is identical to the relaxation sounders mentioned in the previous subsection. It consists of a transmitter and a receiver immersed in the plasma, which excites the plasma in such a way as to make it oscillate at the various magnetoionic frequencies, as described by Benson and Vinas (1988). Other sensors include the *Langmuir probe* and its derivatives, *mass spectrometers*, *particle detectors*, and *magnetic* and *electric-field instruments* (see pp. 49–58 of Hargreaves, 1992).

4.3.5 Capabilities and limitations

Each of the three techniques (involving RBEs, topside sounders and *in situ* probes) discussed in this section does some things very well and other things not so well. However, when these three techniques are employed together in campaigns, they provide considerable information about the ionospheric plasma. Table 4.7 attempts to summarize the salient capabilities of these techniques.

4.4 Other techniques

The techniques discussed in this section are no less important than those discussed in previous sections. However, some of them are variants of certain basic methods, whereas others are quite new and in the process of being implemented.

4.4.1 HF spaced-receiver and Doppler systems

Unfortunately, there is some confusion between the spaced-receiver technique (SRT) and Doppler techniques for measuring the motion of ionospheric irregularities. This may be due in part to the fact that both techniques use multiple receiving antennas, although the antenna spacing for the Doppler method is usually much less than that in the SRT. The concept of the SRT was conceived by

Ratcliffe and Pawsey (1933) and by Pawsey (1935), and was first applied experimentally by Mitra (1949). Discussions of these techniques were given by Kelley (1989, pp. 431–434), Davies (1990, p. 243–245), Hunsucker (1992, pp. 207–211), and Hargreaves (1992, pp. 300–302), and in some recent papers.

The SRT usually involves one transmitter and several receivers, with the location of the receiving antennas optimally spaced in regard to the horizontal scale-size of the particular ionospheric irregularity to be investigated. Figure 4.26 illustrates the wide range of irregularities in the terrestrial ionosphere.

An extended discussion of the SRT is given by Hargreaves (1992, pp. 300–302) and by Hunsucker (1993, pp. 470–473).

Table 4.7. *Advantages and limitations of radio beacons and topside sounders*

Technique	Advantages	Limitations
Radio beacons for TEC studies	Global coverage of the ionosphere from polar-orbiting satellites; constant beacon parameters; not-too-complex receiving system; continuous coverage for a large area from geostationary satellites; ability to study TIDS.	(1) Relatively expensive; (2) rather complex calibration problems; yields a *vast quantity* of data (sometimes overwhelming!); also, rather painstaking data analysis is required. At present, there are few RBEs suitable for ionospheric studies; (3) the polar-orbiting satellites are, of course, always moving in reference to the Earth station, thus convoluting spatial and temporal effects.
Radio beacons for scintillation studies	The averages of global and temporal coverage listed above also apply to the polar-orbiting and geostationary satellites, respectively, used in scintillation studies. *Many* earth stations can use the same beacon for TEC and scintillation studies.	Interpretation of these data in the context of extant theories is a non-trivial task. Remarks 1, 2, and 3 above also apply.
Topside sounders	Since all topside sounders use relatively high-inclination orbits, they have good global coverage. They are also free from D-layer absorption effects, and provide much information on the ionospheric above the F2 peak.	More-complex instrumentation than most beacons.

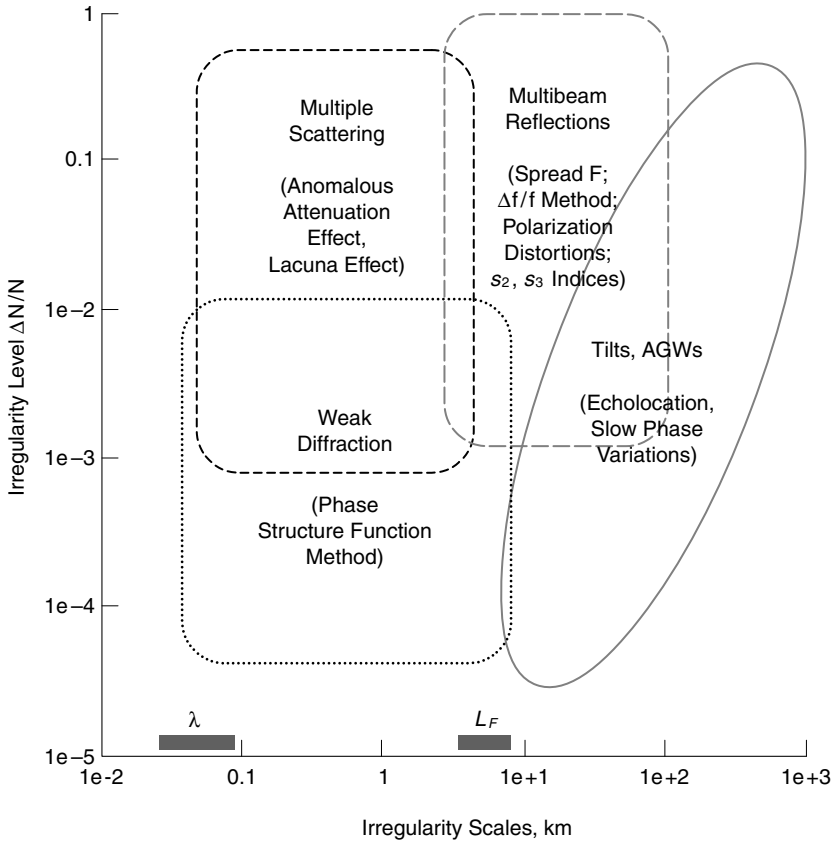

Figure 4.26. A composite spectrum summarizing the intensity of ionospheric irregularities as a function of wavenumber, over a large spatial scale (after Booker, 1979).

4.4.2 The HF Doppler technique

This technique is quite useful for monitoring small, transient changes in the ionosphere. It has been incorporated into several of the modern digital ionosondes and coherent radars, as well as being used as a "stand-alone" technique. Basically, in its first implementation, this technique used a very stable transmitter and one or more stable receivers and local oscillators. These heterodyned the received skywave signal and then the beat frequency was usually recorded on tape at slow speed. The data tapes were then speeded up by a factor of several thousand and the amplitude and phase of the Doppler variation with time were spectrum analyzed. This version of the stand-alone HF/CW Doppler sounder was pioneered in Boulder, Colorado in the early 1960s (Watts and Davies, 1960; Davies, 1962; Davies and Baker, 1966). Modern Doppler techniques utilize digital signal processing and computers instead of tape recorders. A thorough treatment of ionospheric phase and frequency variations and of the HFD technique was given by Davies (1969), and other descriptions may be found in Jones (1989, Chapter 4, pp.

383–398); the *WITS Handbook*, edited by Liu; Hunsucker (1991, pp. 211–213); Hargreaves (1992, pp. 66–67); and Haldoupis and Schlegel (1993).

4.4.3 Ionospheric imaging

For over four decades now, ionospheric physicists and engineers have discussed and used radio methods to image the ionosphere. Rogers (1956) was probably the first to suggest using the wavelength-reconstruction method for this purpose. Schmidt (1972) proposed using VHF signals from a satellite to localize ionospheric irregularities, and a description of a two-dimensional technique was given by Parthasarathy (1975) and Schmidt and Taurianen (1975). Stone (1976) developed a more sophisticated holographic radio camera, using a 32-element antenna array oriented perpendicular to the path of the beacon satellite, with which he produced three-dimensional reconstructions from measured data. Additional details concerning the development of radio-imaging techniques (including computerized ionospheric tomography) from c. 1975 to the present may be found in Nygren *et al.* (1997), Pryse and Kersley (1992), and in reviews by Hunsucker (1993 and 1999) and Kunitsyn and Tereschenko (1992).

4.5 Summary

As we move into the twenty-first century, we see an extensive deployment of state-of-the-art, sophisticated ground- and space-based radio installations for probing the terrestrial ionosphere – probably surpassing the deployment during the IGY/IGC. There has also been a *sea change* in the availability of near-realtime and archived data from these radio installations on the internet. Ionospheric scientists thus have rapid access to an unprecedented assemblage of data as well as using email to rapidly communicate with the principal investigators of the various observatories.

There is now a global distribution of modern ground-based instruments such as digital ionosondes, coherent VHF/UHF radars (CUPRI, COSCAT, STARE, SABRE CANOPUS, . . .), incoherent-scatter radars (EISCAT, Millstone Hill, Jicamarca, Arecibo, MU Radar, and Russian installations), imaging riometers (IRIS), and ionospheric HF heaters (HIPAS, HAARP, Arecibo, EISCAT, . . .). For the first time, we now have near-realtime access to solar, interplanetary, and magnetospheric data from a new generation of scientific satellites such as ACE, WIND, POLAR, and FAST.

When one is analyzing data from these instruments located at high latitude, one must remember that there are some limitations – especially for those using HF. Under especially disturbed conditions (magnetic storms, etc.) ionosondes may be strongly affected by D-region absorption and intense E-region ionization, and HF radars may also be affected by these phenomena.

An invaluable compilation of details of and data from most of the radio techniques listed in this chapter is contained in the CEDAR (Coupling, Energetics and Dynamics of Atmospheric Regions) Data Base published by the National Center for Atmospheric Research (NCAR) in Boulder, Colorado. CEDAR is a program sponsored by the US National Research Foundation (NSF) which sponsors many research programs at institutions in the USA, holds an annual meeting in June in Boulder, Colorado, and updates its data catalog.

4.6 References and bibliography

Section 4.1

Hargreaves, J. K. (1992) *The Solar–Terrestrial Environment*. Ch. 3, Techniques for observing geospace. Cambridge University Press, Cambridge.

Hunsucker, R. D. (1991) *Radio Techniques for Probing the Terrestrial Ionosphere – Physics and Chemistry in Space, Vol. 22 – Planetology*. Springer-Verlag, Berlin.

Hunsucker, R. D. (1993) A review of ionospheric radio techniques: present status and recent innovations, Ch. 22. In *The Review of Radio Science, 1990–1992* (ed. W. R. Stone). Published for the International Union of Radio Science (URSI) by Oxford University Press, Oxford.

Hunsucker, R.D. (1999) Electromagnetic waves in the ionospheric. In *Wiley Encyclopedia of Electrical and Electronic Engineering* (ed. J. Webster), Vol. 6, pp. 494–506. Wiley, New York.

Kelley, M. C. (1989) Appendix A – ionspheric measurement techniques. In *The Earth's Ionosphere – Plasma Physics and Electrodynamics*. Academic Press, New York.

Liu, C.-H. (1989) *World Ionosphere/Thermosphere Study*. WITS Handbook, Vol. 2, Instrumentation. SCOSTEP, University of Illinois Champaign-Urbana, Illinois

Section 4.2

Appleton, E. V. and Barnett, M. A. F. (1925) On some direct evidence for the downward atmospheric reflection of radio waves. *Proc R. Soc.* A **109**, 621–641.

Bailey, V. A. (1937) Interaction by resonance of radio waves. *Nature* **139**, 68–69.

Baker, K. B., Greenwald, R. A., and Ruohoniemi, J. M. (1989) PACE: Polar Anglo-American conjugate experiment. *Eos* **22**, 785–799.

Barnum, J. R. (1986) Ship detection with a high-resolution HF skywave radar. *IEEE J. Oceanic Eng.* **11**, 196.

Belrose, J. S. and Burke, M. J. (1964) Study of the lower ionosphere using partial reflection. *J. Geophys. Res.* **69**, 2779–2818.

Belrose, J. S. (1970) Radio wave probing of the ionosphere by the partial reflection of radio waves (from heights below 100 km). *J. Atmos. Terr. Phys.* **32**, 567–596.

Booker, H. G. (1979) The role of acoustic gravity waves in the generation of spread-F and ionospheric scintillations. *J. Atmos. Terr. Phys.* **41**, 501–515.

Breit, G. and Tuve, M. A. (1926) A test of the existence of the conducting layer. *Phys. Rev.* **28**, 554.

Briggs, B. H. and Vincent, R. A. (1992) Spaced antenna analysis in the frequency domain. *Radio Sci*., **27**, 117–129.

Brookner, (1987) Array radars: an update. *Microwave J*., February, 117–137.

Butt, A. G. (1933) *World Radio*, April, 28.

Carlson, H. C. and Duncan, L. M. (1977) HF excited instabilities in space plasmas. *Radio Sci*., **12**, 1001.

Croft, T. A. (1972) Skywave backscatter: a means for observing our environment at great distance. *Rev. Geophys. Space Phys.* **10**, 73–155.

Davies, K. (1990), Ch. 4, Radio soundings of the ionosphere. In *Ionospheric Radio*, Peter Peregrinus on behalf of the IEE, London.

Detrick, D. L. and Rosenberg, T. J. (1990) A phased-array radiowave imager for studies of cosmic noise absorption. *Radio Sci*. **25**, 325.

Dieminger, W. (1951) The scattering of radio waves. *Proc. Phys. Soc.* B **64**, 142–158.

Evans, J. V. (1969) Theory and practice of ionospheric study by Thomson scatter radar. *Proc. IEEE* **57**, 496.

Ganguli, S., Von Bavel, G., and Brown, A. (1999) Imaging of electron density and magnetic field distributions in the magnetosphere: a new technique. *Proc. IES99*, 563–574.

Gardner, F. F and Pawsey, J.L. (1953) Study of the ionospheric D-region using partial reflections. *J. Atmos. Terr. Phys.* **3**, 321.

Goodman, J. (1992) *HF Communication: Science and Technology*. Van Nostrand Reinhold, New York.

Greenwald, R. A., Weiss, W., Nielson, E., and Thomson, N. R. (1978) Stare: a new radar auroral backscatter experiment in Northern Scandinavia. *Radio Sci.* **13**, 1021–1039.

Greenwald, R. A., Baker, K. B., Hutchins, R.A., and Hanuise, C. (1985) An HF phased array radar for studying small-scale structure in the high-latitude ionosphere. *Radio Sci*. **20**, 63–74.

Greenwald, R.A., Baker, K. B., Dudeney, J. R. Pinnock, M. Jones, T. B., Thomas, E. C., Villain, J.-P., Cerisier, J. C., Senior, C., Hanuise, C., Hunsucker, R. D., Sofko, G., Koehler, J. Nielsen, E., Pellinen, R., Walker, A. D. M., Sato, N., and Yamagishi, H. (1995) The Sapphire North radar experiment: Observation of discrete and diffuse echoes. *Space Sci. Rev.* **71**, 761–796.

Haldoupis, C. and Schlegel, K. (1993) A 50 MHz radio Doppler experiment for mid-latitude E-region coherent backscatter studies. *Radio Sci.* **28**, 959.

Hargreaves, J. K. (1969) Auroral Absorption of HF radio waves in the ionosphere: a review of results from the first decade of riometry. *Proc. IEEE* **57**, 1348–1373.

Kossey, P. A., Turtle, J. P., Pagliarulo, R. P., Klemetti, W. I., and Rasmussen, J. E. (1983) VLF reflection properties of the normal and disturbed polar ionosphere in northern Greenland. *Rad. Sci.*, **18**, 907–916.

Krishnaswamy, S., Detrick, D. L., and Rosenberg, T. J. (1985) The inflection point method of determining riometer quiet day curves. *Radio Sci*. **20**, 123–130.

Kustov, A.V., Koehler, J. A., Sofko, G. J., and Danskin, D. W. (1996) The SAPPHIRE-North radar experiment: Observations of discrete and diffuse echoes. *J. Geophys. Res.*, **101**, 7973–7986.

Kustov, A.V., Koehler, J. A., Sofko, G. J., Danskin, D. W., and Schiffler, A. (1997) Relationship of the SAPPHIRE -North merged velocity and the plasma convection velocity derived from simultaneous SuperDARN radar measurements. *J. Geophys. Res.* **102**, 2495–2501.

Machin, K. E., Ryle, M., and Vomberg, D. D. (1952) The design of an equipment for measuring small radio-frequency noise powers, *Proc.IEE* **99**, 127.

McCrea, K., Schlegel, K., Nygren, T., and Jones, T. B. (1991) COSCAT, A new auroral radar facility on 930 MHz – system description and first results. *Ann.Geophysicae* **9**, 461–469

Meek, C. H. and Manson, A. H. (1987) Medium frequency interferometry of Saskatchewan, Canada. *Can J. Phys.* A **35**, 917–921.

Peterson, A. M. (1951) The mechanism of F-layer propagated backscatter. *J Geophys. Res.* **56**, 221–237.

Rawer, K. (1976) *Manual on Ionospheric Absorption Measurements*. World Data Center A for Solar–Terrestrial Physics, Boulder, Colorado.

Ruohoniemi, J. M., Greenwald, R. A., Baker, K. B., Villain, J.-P., Hanuise, C., and Kelly, J. (1989) *J. Geophys. Res*. **13**, 463.

Sahr, J. D. and Lind, F. D. (1997) The Manatash Ridge radar: passive bistatic radar for upper atmospheric radio science. *Radio Sci*. **32**, 2345–2358.

Schlegel, K. (1984) *HF and VHF Coherent Radars for Investigation of the High Latitude Ionosphere*. Max-Planck-Institut für Aeronomie, Katlenburg-Lindau.

Stubbe, P., Kopka, H. and Rietveld, M. T. (1985) Ionospheric modification experiment with the Tromsø heating facility., *J. Atmos. Terr. Phys.* **47**, 1151–1163.

Tellegin, B. D. (1933) Interaction between radio waves? *Nature* **131**, 840.

Tsunoda, R. T., Livingston, R. C., Buoncore, J. J., and McKinley, A. V. (1995) The frequency-agile radar: a multi-functional approach to remote sensing of the ionosphere. *Radio Sci.* **30**, 1623.

Utlaut, W. F. (1970) An ionospheric modification experiment using very high power, high frequency transmission. *J. Geophys. Res.* **73**, 6402–6405.

Wannberg, G., Wolf, I., Vanhainen, L.-G., Koskenniemi, K., Rottger, J., Postila, M., Markkanen, J., Jacobsen, R., Stenberg, A., Larsen, R., Eliassen, S., Heck, S., and Huuskonen, A. (1997) The EISCAT Svalbard radar: A case study in modern incoherent scatter radar system design. *Radio Sci*. **32**, 2283–2307.

Wilkinson, P. (ed.) (1995) *Ionosonde Networks and Stations*. World Data Center A for Solar–Terrestrial Physics, National Geophysical Data Center, Boulder, Colorado.

Wong, A. Y. (1990) Foreword: Ionospheric modification in the polar region (IMPR). *Radio Sci.* **25**, 1249.

Section 4.3

Basu, Su., Basu, Sa., Weber, E. J., and Coley, W. R. (1988) Case-study of polar cap scintillation modeling using DE2 irregularity measurements at 800 km. *Radio Sci*. **23**, 545–553.

Benson, R. F. and Vinas, F. (1988) Plasma instabilities stimulated by HF transmitters in space. *Radio Sci*. **23**, 585–590.

Benson, R. F. (1997) Evidence for the stimulation of field-aligned electron density irregularities on a short time scale by ionospheric topside sounders. *J. Atmos. Solar–Terr. Phys.* **59**, 2281–2293.

Bowhill, S. A. (1958) The Faraday-rotation rate of a satellite radio signal. *J. Atmos. Terr. Phys.* **13**, 175–176.

Browne, I. C., Evans, J.V., Hargreaves, J. K., and Murray, J. A. W. (1956) Radio echoes from the moon. *Proc.Phys.Soc.* B **69**, 901–920.

Burke, G. J. and Poggio, A. J. (1981) *Numerical electromagnetics code (NEC) – Method of Moments.* NOSC, San Diego, California.

Crain, D. J., Sojka, J. J., Schunk, R. W., nd Klobuchar, J. A. (1993) A first-principle derivation of the high-latitude total election context distribution. *Radio Sci.* **28**, 49.

Davies, K. (1962) The measurement of ionospheric drifts by means of a Doppler shift technique. *J. Geophys.Res.* **67**, 4909–4913.

Davies, K. (1969) *Ionospheric Radiowaves*. Blaisdell, Waltham, Massachusetts.

Davies, K. (1980) Recent studies in satellite radio beacon studies with particular emphasis on the ATS-6 radio beacon experiment. *Space Sci. Rev*. **25**, 357–430.

Davies, K. and Baker, D. M. (1966) On frequency variations of ionospherically propagated HF radio signals. *Radio Sci.* **1**, 545–556.

Davies, K., Fritz, R. B., Grubb, R. N., and Jones, J. E. (1975) Some early results from the ATS-6 Radio Beacon experiments. *Radio Sci.* **10**, 785–799.

Doherty, P. H., Decker, D. T., Sultan, P. J., Rich, F. J., Borer, W. S., and Daniell, R. E. (1999) Validation of PRISM: the climatology. *Proc. IES99, pp. 330–339.*

Evans, J. V. (1956) The measurement of electron content of the ionosphere by the lunar radar method. *Proc. Phys. Soc*. B **69**, 953–955.

Farley, D. T., Ierkic, H. M., and Fejer, B. G. (1981) Radar interferometry. A new technique for studying plasma turbulence in the ionosphere. *J. Geophys. Res*. **86**.

Fremouw, E. J., Leadabrand, R. L., and Livingston, R. C. (1978) Early results from the DNA wideband satellite experiment – complex signal scintillation. *Radio Sci*. **13**, 167–187.

Garriott, O. K., Smith, F. L., and Yuen, P. C. (1965) Observations of ionospheric electron content using a geostationary satellite. *Planet. Space Sci*. **13**, 829–838.

Hewish, A. (1952) The diffraction of galactic radio waves as a method of investigating the irregular structure of the ionosphere. *Proc. R. Soc.* A **214**, 494–514.

Hey, J. S., .Parsons, S. J., and Phillips, J. W. (1946) Fluctuations in cosmic radiation at radio frequencies. *Nature* **158**, 234.

Ho, C. M., Mannucci, A. J., Lindqwister, U. J., Pi, X., and Tsuratani, B. T. (1996)

Global ionosphere perturbations monitored by the worldwide GPS network. *Geophys. Res. Lett.* **23**, 3219–3222.

Hunsucker, R. D. and Owren, L. (1962) Auroral sporadic-E ionization. *J. Res. NBS Radio propagation* D **66**, 581–592.

Inhester, W., Baumjohann, B., Greenwald, R. A., and Nielsen, E. (1981) *J. Geophys. Res.* **49**, 155.

Jackson, J. E. (1986) *Alouette-ISIS Program Summary*. NationaL Space Science Data Center/World Data Center A for Rockets and Satellites, NASA/GSFC, Greenbelt, Maryland.

Jackson, J. E. and Kane, J. A. (1959) Measurements of ionospheric electron densities using a RF probe technique. *J. Geophys. Res*. **64**, 8.

Jones, T. B. (1989) The HF Doppler technique for monitoring transient ionospheric disturbances. *WITS Handbook* vol. 22, p. 383.

Jones, T. B., Spracken, C. T., Stewart, C. P., and Thomas, E. C. (1981) SABRE, a UK/German auroral radar. *IEE Conf. Proc.*, **195**, 269–271.

Kunitsyn, V. E., and Tereschenko, E. D. (1992) Radio tomography of the ionosphere. *IEEE Antennas Propagation Mag.* **34**, 22–32.

Little, C. G. (1952) The origin of the fluctuations on galactic radio noise. Ph. D. Thesis, University of Manchester, Manchester.

Little, C. G. and Leinbach, H. (1959) The riometer – a device for the continuous measurement of ionospheric absorption. *Proc. IRE* **47**, 315–320.

Mitra, S. N. (1949) A radio method of measuring winds in the ionosphere. *Proc. IEE* **96**, 441.

Murray, W. A. S. and Hargreaves, J. K. (1954) Lunar radio echoes and the Faraday effect in the ionosphere. *Nature* **173**, 944.

Nygren, T., Markkanen, M., Lehtinen, M., Tereshehrnko, E. D., and Khudukon, B. Z. (1997) Stochastic inversion in ionospheric radiotomography. *Radio Sci.* **32**, 2359–2372.

Parthasarathy, R. (1975) *Ionospheric Photography at Radio Wavelengths*. Geophysical Institute, University of Alaska-Fairbanks, Fairbanks, Alaska.

Pawsey, J. L. (1935) Further investigations of the amplitude variations of downcoming wireless waves. *Proc. Camb. Phil. Soc.* **31**, 125.

Pi, X, Mannucci, A. J., Lindqwister, U. J., and Ho, C. M. (1997) Monitoring of global ionospheric irregularities using the worldwide GPS network. *Geophys. Res. Lett.* **24**, 2283–2286.

Providakes, J. F. (1985) Radar interferometer observations and theory of plasma irregularities in the auroral ionosphere. Ph.D. Thesis, Cornell University.

Pryse, S. E. and Kersley, L. (1992) A preliminary experimental test of ionospheric tomography. *J. Atmos. Terr. Phys.*, **54**, 1007–1012.

Ratcliffe, J. A. and Pawsey, J. L. (1933) A study of the intensity variations of downcoming radio waves. *Proc. Camb. Phil. Soc*. **29**, 301.

Rodgers, G. L. and Ireland, W. (1980) Ionospheric holography I: the holographic interpretation of ionospheric data. *J. Atmos. Terr. Phys.* **42**, 385–396.

Rogers, G. L. (1956) A new method of analyzing ionospheric movement records. *Nature* **177**, 613–614.

Ruohoniemi, J. M. and Greenwald, R. A. (1997) Rates of scattering occurrence in routine HF radar observations during solar cycle maximum. *Radio Sci*. **32**, 1051.

Schmidt, G. (1972) Determination of the height of ionospheric irregularities with the holographic method. *Z. Geophys.* **38**, 891.

Schmidt, G. and Taurianen, A. (1975) The localization of ionospheric irregularities by the holographic method. *J. Geophys. Res.*, **80**, 4313–4324.

Smith, F. G., Little, C. G., and Lovell, A. C. B. (1950) Origin of the fluctuations in the intensity of radio waves from galactic sources. *Nature* **165**, 422–423.

Stone, W. R. (1976) A holographic radio camera technique for the 3D reconstruction of ionospheric inhomogeneities. *J. Atmos. Terr. Phys.* **38**, 583–592.

Swider, W. (1996) E-region time-dependent chemical model. In *STEP Handbook of Ionospheric Models* (ed. R. Schunk). SCOSTEP Secretariat, NOAA/NGDC, Boulder, Colorado.

Taurianen, A. (1982) Application of wave field reconstruction of VHF radio waves in investigating single, isolated ionospheric irregularities. *Radio Sci*. **17**, 684–692.

Watts, J. M. and Davies, K. (1960) Rapid frequency analysis of fading radio signals. *J. Geophys. Res.* **65** 2295–2302.